Transition dynamics in the Λ_sCDM model: Implications for bound cosmic structures

Evangelos A. Paraskevas,[1,*] Arman Çam,[2,†] Leandros Perivolaropoulos,[1,‡] and Özgür Akarsu[2,§]

[1]*Department of Physics, University of Ioannina, GR-45110, Ioannina, Greece*
[2]*Department of Physics, Istanbul Technical University, Maslak 34469 Istanbul, Turkey*

We explore the predictions of Λ_sCDM, a novel framework suggesting a rapid anti–de Sitter (AdS) to de Sitter (dS) vacua transition in the late Universe, on bound cosmic structures. In its simplest version, the cosmological constant Λ_s abruptly switches sign from negative to positive, attaining its present-day value at a redshift of $z_\dagger \sim 2$. The Λ_sCDM model emerges as a promising solution to major cosmological tensions, particularly the H_0 and S_8 tensions, as well as other less definite tensions. A key aspect of our investigation is examining the impact of the abrupt Λ_sCDM model on the formation and evolution of bound cosmic structures. We identify three primary influences: (i) the negative cosmological constant (AdS) phase for $z > z_\dagger$, (ii) the abrupt transition marked by a type-II (sudden) singularity, leading to an abrupt increase in the Universe's expansion rate at $z = z_\dagger$, and (iii) an increased expansion rate in the late Universe under a positive cosmological constant for $z < z_\dagger$, compared to ΛCDM. Utilizing the spherical collapse model, we investigate the nonlinear evolution of bound cosmic structures within the Λ_sCDM framework. We find that the virialization process of cosmic structures and, consequently, their matter overdensity vary depending on whether the AdS-dS transition precedes or follows the turnaround. Specifically, structures virialize with either increased or reduced matter overdensity compared to the *Planck*-ΛCDM model, contingent on the timing of the transition. Additionally, our results demonstrate that the sudden singularity does not result in the dissociation of bound systems. Despite its profound nature, the singularity exerts only relatively weak effects on such systems, thereby reinforcing the model's viability in this context.

I. INTRODUCTION

The current standard model of cosmology, the Lambda–cold dark matter (ΛCDM) model [1], has been remarkably successful in explaining a broad spectrum of cosmological observations [2–8]. However, setting aside the notoriously challenging theoretical issues associated with the cosmological constant Λ [9–14], the era of high-precision cosmology has seen the emergence of multiple discrepancies at various levels of statistical significance. Notably, the so-called H_0 and S_8 tensions, observed when analyzing different data sets within the ΛCDM model framework, suggest that the model might be incomplete [14–22].

The most statistically significant disagreements lie in the values of the Hubble constant, H_0, and the weighted amplitude of matter fluctuations, S_8. Estimations of H_0 show a discrepancy that reaches a significance of 5σ, as seen between the *Planck* cosmic microwave background (CMB) estimate under the ΛCDM assumption [4] and the

local distance ladder measurements by the SH0ES team [23]. Additionally, the S_8 tension within the ΛCDM framework becomes apparent in the differing results obtained from *Planck* CMB data and KiDS-1000 cosmic shear measurements [7], with discrepancies reaching a 3σ level. In particular, estimates from the *Planck*-ΛCDM framework suggest $H_0 = (67.4 \pm 0.5)$ km s^{-1} Mpc^{-1} [4], while the local H_0 measurement by the SH0ES team, using luminosities of Cepheid calibrators and type Ia supernovae, indicates $H_0 = (73.04 \pm 1.04)$ km s^{-1} Mpc^{-1} [23]. The tension in S_8 is highlighted when comparing constraints on S_8 from high-redshift observations, like the *Planck* data (TT, TE, EE + lowE), reporting $S_8 = 0.834 \pm 0.016$ [4], against those from lower-redshift observations, such as weak gravitational lensing ($S_8 = 0.759^{+0.024}_{-0.021}$ [7] and $S_8 = 0.772 \pm 0.022$ [24]) and galaxy clustering ($S_8 = 0.736 \pm 0.051$ [25]), implying that the *Planck* data predict a stronger growth of cosmological perturbations than what dynamical probe observations infer. A consistency test of the *Planck*-ΛCDM framework suggests that S_8 determinations from $f\sigma_8$ constraints increase with effective redshift, showing a $\sim 3\sigma$ tension with the *Planck*-ΛCDM predictions at lower redshifts, but aligning

*e.paraskevas@uoi.gr
†cam21@itu.edu.tr
‡leandros@uoi.gr
§akarsuo@itu.edu.tr

within 1σ at higher redshifts, hinting that the S_8 tension is physical in origin and potentially indicating a breakdown in the standard ΛCDM model [26].

In addressing the H_0 tension, a variety of extensions to the ΛCDM model have been proposed, which can be broadly categorized as follows:

(1) *Early-time models:* These models introduce new physics before recombination ($z \gtrsim 1100$) to reduce the sound horizon scale, thereby increasing the H_0 value. Examples include early dark energy (EDE) [27–32], new EDE [33–35], anti–de Sitter (AdS) EDE [36–38], and modified gravity [39–45]. Also notable is the approach that suggests modification at the inflationary epoch, with oscillations in the inflaton potential [46].

(2) *Intermediate-/late-time models:* These models introduce new physics at intermediate to late times ($0.1 \lesssim z \lesssim 3.0$). Their goal is to adjust the expansion-rate history $H(z)$ to align H_0 predictions with local measurements while remaining consistent with CMB and late-time observational data. Examples include the Λ_sCDM model [47–50] (which posits a rapidly sign-switching cosmological constant Λ_s, from AdS to dS, in the late Universe as conjectured from the findings in graduated dark energy (gDE) [47]), phantom crossing dark energy [51–57], the omnipotent dark energy model [51,56], dynamical DE on top of an AdS background [56,58–60], and (nonminimally) interacting dark energy (IDE) [61–72].[1]

(3) *Ultra late-time models:* These models implement changes in either fundamental physics or stellar physics during the recent past ($z \lesssim 0.01$) [53,83–86].

While our list includes some key examples from the numerous attempts to resolve the H_0 tension through new physics, it is by no means exhaustive. For a comprehensive overview and detailed classification of various approaches, please refer to Refs. [16,18,19]. It is fair to say that, as of now, there is no widely accepted model that is both observationally and theoretically fully satisfactory. Moreover, addressing the H_0 tension while ensuring compatibility with all available data and without exacerbating other, less significant discrepancies such as the S_8 tension remains a challenging task. Currently, only a few models are known to propose simultaneous solutions to both the H_0 and S_8 tensions. Among these, without claiming to be

exhaustive, are the Λ_sCDM model [47–50], New EDE [34,35], inflation with oscillations in the inflaton potential [46], some IDE models [65,67,72], sterile neutrinos with a nonzero masses + dynamical DE [87], DM with a varying equation-of-state parameter [88], and AdS-EDE with ultra-light axion [38]. However, even with an optimistic view, it is difficult to claim that these models currently present a completed theoretical framework. Among them, the Λ_sCDM model stands out for its simplicity, introducing only one extra free parameter compared to the standard ΛCDM model, $z_{\dagger}$, which signifies the redshift of the rapid AdS-dS transition. The remainder of this paper focuses on the Λ_sCDM model.

Another aspect drawing our attention to the Λ_sCDM model is its potential relevance to recent findings from the James Webb Space Telescope (JWST). As initially noted in [49] (refer to Sec. IV C therein), the model's incorporation of a negative (AdS) cosmological constant for $z \gtrsim 2$ could lead to enhanced structure formation at these higher redshifts. This possibility aligns with observations from JWST's deep-space probes ($z \gtrsim 5$), which suggest that structure formation is more intense at these higher redshifts than predicted by the standard ΛCDM framework [89,90]. Specifically, JWST observations have revealed that the early formation of luminous galaxies [90–98] exhibits more intense growth.[2] Moreover, galaxies within the redshift range of $7 \lesssim z \lesssim 10$ display an unusually high star-formation rate [89,101–103] and the observed number density of ultraviolet bright galaxies at redshift $z \sim 15$ exceeds expectations, posing a challenge to the galaxy formation models based on the ΛCDM model [94,104]. Recent works have shown [96,105,106] that the presence of a negative cosmological constant (or, more broadly, negative energy densities contributing to the Friedmann equation) at relevant redshifts can accommodate the anomalous findings on cosmological structures observed by the JWST's deep-space probes.

The Λ_sCDM model exhibits features that can address both the H_0 and S_8 tensions and, potentially, the anomalous findings from the JWST. All of these features are controlled by a single extra free parameter, $z_{\dagger} \sim 1.8$ [49,50], the redshift at which the cosmological constant switches its sign from negative to positive and achieves its present-day value. The mechanism by which the Λ_sCDM model achieves these outcomes is straightforward [48–50]: the presence of a negative cosmological constant for $z > z_{\dagger}$ implies that $H(z)$ is smaller than in ΛCDM at these higher redshifts. Consequently, the smaller $H(z)$, offering less resistance against structure growth, leads to faster structure growth for $z > z_{\dagger}$, aligning with findings from JWST. On the other hand, due to the fact that the comoving angular

---

[1]DE densities that reach negative values, consistent with a negative (AdS-like) cosmological constant, especially for $z \gtrsim 1.5$–2, are also observed in model-independent/nonparametric observational reconstructions [73–82]. Furthermore, a recent model-independent reconstruction of the IDE kernel, employing Gaussian process methods as suggested in [78], reveals that DE assumes negative densities for $z \gtrsim 2$, which suggests that IDE models do not preclude the possibility of negative DE densities at high redshifts.

[2]However, some studies such as those in [99–101] argue that the JWST data are not robust enough to conclusively assert a tension with the ΛCDM model.

diameter distance to the last scattering surface, $D_M(z_*) = c \int_0^{z_*} H^{-1} dz$ (where $z_* \approx 1090$), is strictly determined by the CMB power spectra, any reduction in $H(z)$ for $z > z_\dagger$, compared to ΛCDM, must be compensated by an increase in $H(z)$ for $z < z_\dagger$. This explains both the higher H_0 values predicted by Λ_sCDM and the suppression of structure growth for $z < z_\dagger$, in comparison to ΛCDM, as the larger $H(z)$ for $z < z_\dagger$ implies greater resistance to structure growth. Essentially, Λ_sCDM predicts higher values of both H_0 and σ_8 compared to ΛCDM. However, the decreased value of Ω_{m0}, due to the increased H_0, outweighs the increased σ_8, resulting in a decreased $S_8 = \sigma_8 \sqrt{\Omega_{m0}/0.3}$. Thus, it is conceivable that the Λ_sCDM model can account for intense structure growth at higher redshifts while simultaneously accommodating weaker growth at redshifts $z \lesssim 2$ [24,107–110].

The Λ_sCDM [47–49] model emerges as one of the promising models for addressing major cosmological tensions and stands as the most economical model among those in the literature with this capability. While the abrupt/rapid nature of the Λ_s, along with its shift from negative to positive values, presents challenges in identifying a concrete physical mechanism, the phenomenological success of Λ_sCDM, despite its simplicity, strongly encourages the search for possible underlying physical mechanisms. Furthermore, it could have profound implications in theoretical physics, given that $\Lambda < 0$ is a theoretical sweet spot; the AdS vacuum is welcome due to the AdS/CFT correspondence [111] and is preferred by string theory and string theory–motivated supergravities [112]. Thereby, it would be natural to associate Λ_s with a possible AdS-dS (phase) transition that is derived in such fundamental theories and the theories that find motivation from them. Recently, it was shown in [113] that although the AdS swampland conjecture suggests that Λ_s in the late Universe seems unlikely —due to the AdS vacua being an infinite distance apart from dS vacua in moduli space—it can still be realized through the Casimir forces of fields inhabiting the bulk. Another study [114] demonstrated that in various formulations of general relativity (GR) it is possible to obtain a sign-switching cosmological constant through an overall sign change of the metric. In a more recent study [115], it was demonstrated that within a type-II minimally modified gravity framework, known as VCDM [116,117], an auxiliary scalar field with a linear potential[3] can induce an effective cosmological constant, enabling the realization of an abrupt Λ_sCDM model through a piecewise linear potential with two segments and facilitating smooth Λ_sCDM models by smoothing out this potential. This novel theoretical framework, endowed with a specific Lagrangian from the VCDM theory, elevates Λ_sCDM to a theoretically

complete physical cosmology, offering a fully predictive description of our Universe. These theoretical developments, emerging shortly after the introduction of the Λ_sCDM model, suggest that this model could potentially serve as an alternative to the standard ΛCDM model in the near future.

The simplest version of the Λ_sCDM model is constructed phenomenologically by replacing the usual Λ in the standard ΛCDM model with $\Lambda_s \equiv \Lambda_{s0} \mathrm{sgn}(z_\dagger - z)$, where a cosmological constant undergoes an abrupt sign switch in the past, occurring at redshift $z_\dagger$, and maintains a constant positive value thereafter [48–50]. In this paper, we occasionally refer to this model as the abrupt Λ_sCDM. It is characterized by the following Friedmann equation:

$$\frac{H^2(z)}{H_0^2} = \Omega_{m0}(1+z)^3 + \Omega_{\Lambda_s0} \mathrm{sgn}(z_\dagger - z) + \Omega_{k0}(1+z)^2, \quad (1)$$

where the transition is incorporated using the signum function (sgn) and $\Lambda_{s0} > 0$ represents the present-day value of Λ_s (or for redshifts $z < z_\dagger$).[4] Here, $H(z)$ represents the Hubble parameter, while Ω_{m0}, Ω_{Λ_s0}, and Ω_{k0} denote the present-day density parameters for the pressureless fluid (baryons + CDM), sign-switching cosmological constant, and spatial curvature, respectively. In the abrupt Λ_sCDM model, the Hubble parameter exhibits a discontinuity in the past, specifically, at redshift $z = z_\dagger$, indicative of a-type II (sudden) singularity at this exact redshift [122].[5,6] Although this singularity is mild, being weak enough not to compromise the cosmological model's viability (see Appendix A for further discussion and Refs. [121,125,127,128] for additional reading), it nonetheless imparts a velocity kick to particles. This, in turn, delays the growth of overdensities following the sign switch in the cosmological constant. Thus, compared to the standard model, the Λ_sCDM model enhances early-Universe structure growth, particularly for $z > z_\dagger$, driven by an initially negative cosmological constant. Conversely, in the late Universe ($z < z_\dagger$) when Λ_s becomes positive, it predicts weaker structure growth. This is attributed to a lower Ω_{m0}, a consequence of a larger H_0, in

---

[3]Refer to Refs. [118–120] for discussion on the utilization of a scalar field with a linear potential in the context of DE modeling within the GR framework.

[4]Note that this abrupt behavior of Λ_s, as described and considered in this work, represents an idealized depiction of a rapid transition phenomenon, akin to a phase transition, from AdS vacuum to dS vacuum, or a DE model such as gDE [47] capable of mimicking this behavior [49]. Additionally, it is important to emphasize that Λ_s, whether exhibiting abrupt changes or not, does not violate the principle of energy conservation. For further details on this aspect, see Refs. [49,121].

[5]For a general overview of cosmological singularities, readers are referred to Refs. [122–126].

[6]This singularity is absent in smooth Λ_sCDM models featuring a rapidly yet smoothly occurring sign switch, as realized under the VCDM framework in Ref. [115]. However, this work delves into the effects of Λ_s in its most extreme form, the abrupt Λ_sCDM model, within the GR framework.

comparison to ΛCDM, combined with the added impact of the velocity kick at the transition.

The behavior of spherically symmetric overdensities in a universe dominated by DE has been extensively studied [105,129–139]. The spherical collapse model is a fundamental tool for understanding the evolution of these overdensities within a Friedmann-Robertson-Walker (FRW) cosmology. These overdensities function as "subuniverses" with mean densities exceeding the background matter density. They are influenced by both DE and the expansion dynamics of the FRW background. Despite the universe's overall expansion, these overdensities evolve relatively independently, akin to the evolution of a closed FRW universe [140–144]. Initially expanding with the cosmological background, they eventually succumb to local gravitational forces, leading to a "turnaround" phase. After this turnaround, the regions begin to collapse, a process that, according to GR, would theoretically lead to a singularity. However, from an astrophysical standpoint, virialization is commonly understood to occur before the formation of a singularity, resulting in a stable equilibrium state.

The spherical collapse model encompasses three distinct phases:

(1) *Expansion phase:* Initially, the overdense region expands in tandem with the cosmic background.

(2) *Turnaround:* Eventually, this spherically symmetric region decouples from the cosmic expansion, reaching its maximum radius. Here, local gravitational forces become dominant, initiating the collapse.

(3) *Shell crossing and virialization:* In this final stage, shells within the overdensity undergo gravitational oscillations and interactions, leading to an exchange of gravitational potential energy and ultimately resulting in virialization. This stabilizes the system in a state of equilibrium.

In this study, we utilize the spherical collapse model to investigate the formation and evolution of bound cosmic structures within the abrupt Λ_sCDM model. Our primary objective is to assess the impact of replacing the positive cosmological constant in the ΛCDM model with an abrupt sign-switching cosmological constant. This exploration involves analyzing the effects of (i) a past negative cosmological constant (AdS) phase for $z > z_\dagger \sim 2$, (ii) the abrupt transition itself, characterized by a sudden jump in the expansion rate of the Universe—a type-II (sudden) singularity—at $z = z_\dagger$, and (iii) the increased expansion rate of the Universe in the Λ_sCDM model for $z < z_\dagger$. Notably, aside from the faster expansion rate, the Λ_sCDM and ΛCDM models are identical for $z < z_\dagger$. Our investigation focuses on the densities and scales of virialized structures, characterized by their virial and turnaround radii, across various turnaround redshifts z_{ta} while accounting for the sign switch in the cosmological constant in the late Universe. We identify three primary transition scenarios

based on the timing of Λ_s's sign switch, i.e., the AdS-dS transition, relative to the evolutionary stage of the overdensities: two occurring before virialization ($a_\dagger < a_{vir}$), specifically, before turnaround ($a_\dagger < a_{ta} < a_{vir}$) and after turnaround ($a_{ta} < a_\dagger < a_{vir}$), and a third scenario where the transition occurs post-virialization ($a_{vir} < a_\dagger$).

In this paper, we first revisit the spherical collapse model with a cosmological constant of arbitrary sign, employing a semi-Newtonian framework. We derive virialized densities, building upon the methodology presented in earlier work [105] (Sec. II). We then extend our analysis to the Λ_sCDM model [47–50], incorporating transitional effects of the cosmological constant into our calculations (Sec. III). Our results include derived virialized densities in the Λ_sCDM model, which we compare with those in the ΛCDM model. In particular, this analysis focuses on the transition marked by a sudden cosmological singularity [122]. Last, employing the Newtonian approximation of a bound system within an expanding background [145–148], we examine the impact of this sudden singularity on systems that virialized before the transition (Sec. IV).

II. SPHERICAL COLLAPSE MODEL IN THE PRESENCE OF A COSMOLOGICAL CONSTANT

In this section, we focus on calculating virialized densities and radii using the turnaround overdensity (δ_{ta}) in the presence of a cosmological constant [105,137]. Building upon the methodology and results presented here, we analyze the Λ_sCDM model in the next section.

A. Expansion phase

1. Background Universe

In our analysis, we use $R(t)$ to represent the local scale factor within the spherical overdensity and R_p for the physical radius, defined as $R_p \equiv R(t)\chi_0$, where χ_0 is the corresponding comoving radius. The notation ρ_m denotes the (pressureless) matter energy density of the spherical overdensity and $\tilde{\rho}_m$ denotes the matter energy density of the background Universe. The overdensity at a given cosmic epoch, characterized by the background scale factor a, is described as

$$\delta(a) = \frac{\rho_m(a) - \tilde{\rho}_m(a)}{\tilde{\rho}_m(a)}. \qquad (2)$$

At the turnaround time, denoted as t_{ta}, the background scale factor reaches $a_{ta} \equiv a(t_{ta})$. Simultaneously, the scale factor of the overdense region attains its maximum value, denoted as $R_{ta} \equiv R(t_{ta})$, resulting in its maximum physical size $R_{p,ta} \equiv R_{ta}\chi_0$.

The evolution of the scale factor of the perturbation, $R(t)$, and the scale factor of the background, $a(t)$, are governed by their respective Friedmann equations. These

equations incorporate the effects of spatial curvature, matter density, and the cosmological constant within the spherical overdensity. The Friedmann equation for the background Universe is provided in the following form [133,136,137,144]:

$$\frac{\dot{a}^2}{a^2} = \frac{8\pi G}{3}\tilde{\rho}_{m0}(a^{-3} + \omega + \xi a^{-2}), \qquad (3)$$

where ω and ξ are defined as

$$\omega \equiv \frac{\rho_{\Lambda 0}}{\tilde{\rho}_{m0}} = \frac{\Omega_{\Lambda 0}}{\Omega_{m0}},$$

$$\xi \equiv \frac{\tilde{\rho}_{crit,0} - \tilde{\rho}_{m0} - \rho_{\Lambda 0}}{\tilde{\rho}_{m0}} = \frac{1}{\Omega_{m0}} - 1 - \omega. \qquad (4)$$

2. Overdensity

Let us define an initial comoving time t_i, which is the moment when the scale factors and their time derivatives for both the background Universe and the overdense region are the same:

$$a_i = R_i, \qquad \dot{a}_i = \dot{R}_i. \qquad (5)$$

With these initial conditions, we reformulate the Friedmann equations for the local overdensity and the background as follows:

$$\frac{\dot{R}^2}{R^2} = \frac{8\pi G}{3}\rho_{m,i}\left(R^{-3} + \frac{\rho_{\Lambda,i}}{\rho_{m,i}} - \bar{\kappa}R^{-2}\right), \qquad (6)$$

$$\frac{\dot{a}^2}{a^2} = \frac{8\pi G}{3}\tilde{\rho}_{m,i}\left(a^{-3} + \frac{\rho_{\Lambda,i}}{\tilde{\rho}_{m,i}} + \bar{\xi}a^{-2}\right). \qquad (7)$$

We define the parameters corresponding to the spatial curvatures of both the spherically overdense region and the cosmological background at time t_i as

$$\bar{\kappa} \equiv \frac{\rho_{m,i} + \rho_{\Lambda,i} - \rho_{crit,i}}{\rho_{m,i}},$$

$$\bar{\xi} \equiv \frac{\tilde{\rho}_{crit,i} - \tilde{\rho}_{m,i} - \rho_{\Lambda,i}}{\tilde{\rho}_{m,i}}. \qquad (8)$$

From Eq. (5), we infer that the critical densities at time t_i for both the overdense region and the cosmological background are identical:

$$\rho_{crit,i} \equiv \frac{3}{8\pi G}\frac{\dot{R}_i^2}{R_i^2}, \qquad \tilde{\rho}_{crit,i} \equiv \frac{3}{8\pi G}\frac{\dot{a}_i^2}{a_i^2}. \qquad (9)$$

Assuming that $-\bar{\kappa} = \bar{\xi}$ at that initial moment and $\rho_{crit,i} = \tilde{\rho}_{crit,i}$, this leads to the relationship $\rho_{m,i} = \tilde{\rho}_{m,i}$. Subsequently, we can express the overdensity as

$$\rho_m(a) = \tilde{\rho}_{m,i}R^{-3}(a). \qquad (10)$$

Equations (2) and (10), evaluated at the moment t_i, yield

$$R^{-3}(a) = a^{-3}[1 + \delta(a)]. \qquad (11)$$

Given that $\tilde{\rho}_{m,i} = \tilde{\rho}_{m0}a_i^{-3}$ and applying the rescaling transformations $a_i R \rightarrow R$ and $\bar{\kappa}/a_i \rightarrow \kappa$, Eq. (6) is rewritten as [129,133,137,139]

$$\frac{\dot{R}^2}{R^2} = \frac{8\pi G}{3}\tilde{\rho}_{m0}(R^{-3} + \omega - \kappa R^{-2}), \qquad (12)$$

which is the Friedmann equation for the local overdensity with scale factor $R(t)$. By dividing Eq. (12) by Eq. (3) and taking the square root, we deduce that

$$\frac{dR}{da} = \pm\sqrt{\frac{a}{R}\frac{1 + \omega R^3 - \kappa R}{1 + \omega a^3 + \xi a}}. \qquad (13)$$

This equation describes the dynamics of the overdensity, where the positive branch corresponds to expansion (pre-turnaround) and the negative branch indicates contraction (post-turnaround).

B. Turnaround

We can determine the physical size of the overdensity at the turnaround, denoted as $R_{p,ta}$, using the criterion

$$\left.\frac{dR}{da}\right|_{a=a_{ta}} = 0. \qquad (14)$$

This condition consequently establishes the relationship between κ, ω, and R_{ta}:

$$\kappa = (1 + \omega R_{ta}^3)R_{ta}^{-1}. \qquad (15)$$

By rearranging the corresponding terms on each side of the positive branch of Eq. (13), which represents the expansion phase of the overdensity, and considering Eq. (15), we derive

$$\int_0^R dR\sqrt{\frac{R}{1 + \omega R^3 - [(1 + \omega R_{ta}^3)R_{ta}^{-1}]R}}$$

$$= \int_0^a da\sqrt{\frac{a}{1 + \omega a^3 + \xi a}}. \qquad (16)$$

In Eq. (16), employing transformation of variables such that on the lhs $u = R/R_{ta}$ and on the rhs $y = a/a_{ta}$, we obtain

$$\int_0^1 du \sqrt{\frac{u}{a_{ta}^{-3}(1+\delta_{ta})(1-u) - \omega u(1-u^2)}}$$
$$= \int_0^1 dy \sqrt{\frac{y}{a_{ta}^{-3} + \omega y^3 + \xi a_{ta}^{-2} y}}. \tag{17}$$

Thus, for given values of ξ, ω, and a_{ta}, we can calculate the density contrast at the turnaround, denoted as δ_{ta}.

C. Shell crossing and virialization

1. Gravitational potential of the halo

Drawing from the contributions of [149–152], we characterize the gravitational potential energy of a system composed of both DE and DM, noting that virialization is exclusive to the DM component. The gravitational potential energy of the halo system can be represented as

$$\mathcal{U}_{halo} = \frac{1}{2}\int_V \rho_{DM}\Phi_{DM} dV + \int_V \rho_{DM}\Phi_{DE} dV. \tag{18}$$

The gravitational potentials of DM (Φ_{DM}) and DE (Φ_{DE}) can be written as (see Appendix B for the derivation)

$$\Phi_{DM}(r) = \begin{cases} -2\pi G\rho_{DM}(R^2 - r^2/3), & r < R, \\ -4\pi G\rho_{DM}R^3/3r, & r \geq R, \end{cases}$$
$$\Phi_{DE}(r) = 2\pi G\rho_{DE}(1 + 3w_{DE})\frac{r^2}{3}. \tag{19}$$

Considering a homogeneous spherical distribution of DM with a physical radius R_p and mass M, the energy densities of DM and DE are given by

$$\rho_{DM} \equiv 3M/4\pi R_p^3,$$
$$\rho_{DE} \equiv \rho_{DM} e_{DE}\left(\frac{a}{a_{ta}}\right)^{-3(1+w_{DE})}\left(\frac{R_p}{R_{p,ta}}\right)^3, \tag{20}$$

where e_{DE} represents the ratio of the densities at the turnaround:

$$e_{DE} \equiv \frac{\rho_{DE}(a_{ta})}{\rho_{DM}(a_{ta})}. \tag{21}$$

Thus, the integrals over the volume of $\rho_{DM}\Phi_{DM}$ and $\rho_{DM}\Phi_{DE}$, considering Eqs. (19)–(21), read as follows:

$$\frac{1}{2}\int_V \rho_{DM}\Phi_{DM} dV = -\frac{3}{5}\frac{GM^2}{R_p},$$
$$\int_V \rho_{DM}\Phi_{DE} dV = -\frac{3}{5}\frac{GM^2}{R_p}\Theta_{DE}\left(\frac{a}{a_{ta}}\right)^{-3(1+w_{DE})}\left(\frac{R_p}{R_{p,ta}}\right)^3, \tag{22}$$

where $\Theta_{DE} \equiv -\frac{1}{2}(1 + 3w_{DE})e_{DE}$. Consequently, by following Eq. (18), the potential energy of the system can be expressed as

$$\mathcal{U}_{halo} = -\frac{3}{5}\frac{GM^2}{R_p}\left[1 + \Theta_{DE}\left(\frac{a}{a_{ta}}\right)^{-3(1+w_{DE})}\left(\frac{R_p}{R_{p,ta}}\right)^3\right]. \tag{23}$$

2. Virialization condition

The conservation of energy, from the moment of the turnaround until the virialization stage, implies

$$\mathcal{E} \equiv \mathcal{U}_{halo}\Big|_{R_p = R_{p,ta}} = (\mathcal{K}_{halo} + \mathcal{U}_{halo})\Big|_{R_p = R_{p,vir}}. \tag{24}$$

Assuming that the virial theorem holds, the kinetic energy can be written as

$$\mathcal{K}_{halo} = \frac{R_p}{2}\frac{d\mathcal{U}_{halo}}{dR_p} \tag{25}$$

and, given Eq. (25), Eq. (24) suggests the virialization condition

$$\mathcal{U}_{halo}|_{R_p = R_{p,ta}} = \left(\frac{R_p}{2}\frac{d\mathcal{U}_{halo}}{dR_p} + \mathcal{U}_{halo}\right)\Big|_{R_p = R_{p,vir}}. \tag{26}$$

For a potential given in Eq. (23), Eq. (26) can be recast as

$$4\Theta_{DE}\alpha_{DE}\eta^3 - 2(1 + \Theta_{DE})\eta + 1 = 0, \tag{27}$$

where η and α_{DE} are defined through

$$\eta \equiv \frac{R_{p,vir}}{R_{p,ta}}, \qquad \alpha_{DE} \equiv \left(\frac{a_{vir}}{a_{ta}}\right)^{-3(1+w_{DE})}. \tag{28}$$

The solution of Eq. (27) expanded in terms of Θ_{DE} can be expressed by [105,134,135,149–155]

$$\eta = \frac{1}{2} + \frac{1}{4}\Theta_{DE}(-2 + \alpha_{DE})$$
$$+ \frac{1}{8}\Theta_{DE}^2(-2 + \alpha_{DE})(-2 + 3\alpha_{DE}) + \dots \tag{29}$$

In the specific case of a positive cosmological constant ($w_\Lambda = -1$) as the DE component, implying $\alpha_\Lambda = 1$ and $\Theta_\Lambda = e_\Lambda$, Eq. (27) can be written as

$$4e_\Lambda\eta^3 - 2(1 + e_\Lambda)\eta + 1 = 0. \tag{30}$$

This can be approximated by

$$\eta = \frac{1}{2} - \frac{e_\Lambda}{4} - \frac{e_\Lambda^2}{8} + \dots, \tag{31}$$

where the parameter $e_\Lambda \equiv \omega a_{\text{ta}}^3/(1 + \delta_{\text{ta}})$, obtained from Eq. (21).

3. Density contrast at the virialization

Given that $t_{\text{vir}} = 2t_{\text{ta}}$ and assuming the collapse is completed at $t = t_{\text{vir}}$, Eq. (3) leads to

$$\int_0^{y_{\text{vir}}} \mathrm{d}y \sqrt{\frac{y}{a_{\text{ta}}^{-3} + \omega y^3 + \xi a_{\text{ta}}^{-2} y}}$$
$$= 2 \int_0^1 \mathrm{d}y \sqrt{\frac{y}{a_{\text{ta}}^{-3} + \omega y^3 + \xi a_{\text{ta}}^{-2} y}}, \quad (32)$$

where $y_{\text{vir}} \equiv a_{\text{vir}}/a_{\text{ta}}$. Therefore, given specific values of ξ, ω, and a_{ta}, we can use Eq. (32) to compute the scale factor at virialization, a_{vir}. Subsequently, the value of δ_{vir} can be calculated using the following relation:

$$1 + \delta_{\text{vir}} = (1 + \delta_{\text{ta}})\left(\frac{y_{\text{vir}}}{\eta}\right)^3. \quad (33)$$

III. Λ_sCDM: Λ_s-SIGN SWITCH BEFORE VIRIALIZATION

Within the Λ_sCDM [48–50] framework, the evolution of the background Universe is governed by

$$\frac{\dot{a}^2}{a^2} = \frac{8\pi G}{3}\tilde{\rho}_{\text{m}0}[a^{-3} + \omega_s \text{sgn}(1/a_\dagger - 1/a) + \xi_s a^{-2}], \quad (34)$$

whereas the evolution for the overdensity is described by

$$\frac{\dot{R}^2}{R^2} = \frac{8\pi G}{3}\tilde{\rho}_{\text{m}0}[R^{-3} + \omega_s \text{sgn}(1/a_\dagger - 1/a) - \kappa_s R^{-2}], \quad (35)$$

where ω_s and ξ_s are parameters defined as

$$\omega_s \equiv \frac{\rho_{\Lambda_s 0}}{\tilde{\rho}_{\text{m}0}} = \frac{\Omega_{\Lambda_s 0}}{\Omega_{\text{m}0}},$$

$$\xi_s \equiv \frac{\tilde{\rho}_{\text{crit},0} - \tilde{\rho}_{\text{m}0} - \rho_{\Lambda_s 0}}{\tilde{\rho}_{\text{m}0}} = \frac{1}{\Omega_{\text{m}0}} - 1 - \omega_s.$$

After dividing Eq. (34) by Eq. (35), we obtain

$$\frac{\mathrm{d}R}{\mathrm{d}a} = \pm \sqrt{\frac{a}{R}\frac{1 + \omega_s \text{sgn}(1/a_\dagger - 1/a)R^3 - \kappa_s R}{1 + \omega_s \text{sgn}(1/a_\dagger - 1/a)a^3 + \xi_s a}}. \quad (36)$$

A. Λ_s-sign switch before the turnaround ($a_\dagger < a_{\text{ta}} < a_{\text{vir}}$)

1. Density contrast at the turnaround

Assuming that the Λ_s-sign switch transition occurs during the expansion phase of the overdensity, we integrate Eq. (36) as follows:

$$\int_0^R \mathrm{d}R \sqrt{\frac{R}{1 + \omega_s \text{sgn}(1/a_\dagger - 1/a)R^3 - \kappa_s R}}$$
$$= \int_0^a \mathrm{d}a \sqrt{\frac{a}{1 + \omega_s \text{sgn}(1/a_\dagger - 1/a)a^3 + \xi_s a}}. \quad (37)$$

By implementing the changes of variables $u = R/R_{\text{ta}}$ on the lhs of Eq. (37) and $y = a/a_{\text{ta}}$ on the rhs of Eq. (37), and integrating until the turnaround moment, we obtain the following system of equations:

$$\int_0^{y_\dagger} \mathrm{d}y \sqrt{\frac{y}{a_{\text{ta}}^{-3} - \omega_s y^3 + \xi_s a_{\text{ta}}^{-2} y}}$$
$$= \int_0^{u_\dagger} \mathrm{d}u \sqrt{\frac{u}{a_{\text{ta}}^{-3}(1 + \delta_{\text{ta}})(1 - u) - \omega_s u(1 + u^2)}}, \quad (38)$$

$$\int_{y_\dagger}^1 \mathrm{d}y \sqrt{\frac{y}{a_{\text{ta}}^{-3} + \omega_s y^3 + \xi_s a_{\text{ta}}^{-2} y}}$$
$$= \int_{u_\dagger}^1 \mathrm{d}u \sqrt{\frac{u}{a_{\text{ta}}^{-3}(1 + \delta_{\text{ta}})(1 - u) - \omega_s u(1 - u^2)}}. \quad (39)$$

Here we have denoted $y_\dagger \equiv a_\dagger/a_{\text{ta}}$, $u_\dagger \equiv R_\dagger/R_{\text{ta}}$, and $\kappa_s = (1 + \omega_s R_{\text{ta}}^3)R_{\text{ta}}^{-1}$, given that the cosmological constant is positive at the moment of turnaround. Thus, for a given $y_\dagger$, we can derive the corresponding values of $u_\dagger$ and δ_{ta} that satisfy Eqs. (38) and (39) simultaneously.

2. Density contrast at the virialization

In such a case, the Λ_s-sign switch transition occurs prior to the turnaround moment. As a result, at the turnaround, the cosmological constant has already been positive, ensuring that the collapse proceeds with a positive cosmological constant throughout, similar to the ΛCDM case. At the moment of turnaround,

$$\frac{\rho_{\Lambda_s}(a_{\text{ta}})}{\rho_{\text{m}}(a_{\text{ta}})} = \text{sgn}(1/a_\dagger - 1/a_{\text{ta}})e_\Lambda \equiv e_{\Lambda_s}, \quad (40)$$

where we have defined

$$e_{\Lambda_s} \equiv \omega_s a_{\text{ta}}^3/(1 + \delta_{\text{ta}}). \quad (41)$$

The virialization condition results in

$$4e_{\Lambda_s}\eta^3 - 2(1 + e_{\Lambda_s})\eta + 1 = 0, \quad (42)$$

which can be approximated by

$$\eta = \frac{1}{2} - \frac{e_{\Lambda_s}}{4} - \frac{e_{\Lambda_s}^2}{8} + \cdots \quad (43)$$

Assuming that the collapse is completed at $t = t_{\mathrm{vir}}$ (with $t_{\mathrm{vir}} \simeq 2t_{\mathrm{ta}}$), the Friedmann equation for the background universe (for $y_{\dagger} < 1$) is given by

$$
\int_0^{y_{\dagger}} dy \sqrt{\frac{y}{a_{\mathrm{ta}}^{-3} - \omega_s y^3 + \xi_s a_{\mathrm{ta}}^{-2} y}}
$$
$$
+ \int_{y_{\dagger}}^{y_{\mathrm{vir}}} dy \sqrt{\frac{y}{a_{\mathrm{ta}}^{-3} + \omega_s y^3 + \xi_s a_{\mathrm{ta}}^{-2} y}}
$$
$$
= 2\left(\int_0^{y_{\dagger}} dy \sqrt{\frac{y}{a_{\mathrm{ta}}^{-3} - \omega_s y^3 + \xi_s a_{\mathrm{ta}}^{-2} y}} \right.
$$
$$
\left. + \int_{y_{\dagger}}^1 dy \sqrt{\frac{y}{a_{\mathrm{ta}}^{-3} + \omega_s y^3 + \xi_s a_{\mathrm{ta}}^{-2} y}} \right). \tag{44}
$$

From Eq. (44), we deduce that

$$
\int_1^{y_{\mathrm{vir}}} dy \sqrt{\frac{y}{a_{\mathrm{ta}}^{-3} + \omega_s y^3 + \xi_s a_{\mathrm{ta}}^{-2} y}}
$$
$$
= \int_0^{y_{\dagger}} dy \sqrt{\frac{y}{a_{\mathrm{ta}}^{-3} - \omega_s y^3 + \xi_s a_{\mathrm{ta}}^{-2} y}}
$$
$$
+ \int_{y_{\dagger}}^1 dy \sqrt{\frac{y}{a_{\mathrm{ta}}^{-3} + \omega_s y^3 + \xi_s a_{\mathrm{ta}}^{-2} y}}. \tag{45}
$$

Thus, it becomes feasible to deduce the value of a_{vir} in terms of a_{ta} and subsequently δ_{vir} from Eq. (33).

B. Λ_s-sign switch after the turnaround ($a_{\mathrm{ta}} < a_{\dagger} < a_{\mathrm{vir}}$)

1. Density contrast at the turnaround

Given that the transition occurs after the turnaround (i.e., $a_{\dagger} > a_{\mathrm{ta}}$), the expansion phase persists with a negative cosmological constant throughout. The value of δ_{ta} is determined using the following equation:

$$
\int_0^1 du \sqrt{\frac{u}{a_{\mathrm{ta}}^{-3}(1 + \delta_{\mathrm{ta}})(1 - u) + \omega_s u(1 - u^2)}}
$$
$$
= \int_0^1 dy \sqrt{\frac{y}{a_{\mathrm{ta}}^{-3} - \omega_s y^3 + \xi_s a_{\mathrm{ta}}^{-2} y}}, \tag{46}
$$

which corresponds to Eq. (17), with the substitution of $\omega \rightarrow -\omega_s$.[7] Note that have used the relation $\kappa_s = (1 - \omega_s R_{\mathrm{ta}}^3) R_{\mathrm{ta}}^{-1}$, where the cosmological constant is negative at the moment of turnaround.

---

[7]We have also assumed that $a_{\mathrm{ta}} \lesssim a_{m\Lambda_s} \equiv (\Omega_{m0}/\Omega_{\Lambda_s 0})^{\frac{1}{3}}$, i.e., the moment where $H^2(a_{m\Lambda_s}) = 0$.

2. Effect of the type-II singularity: Free particle in the Hubble flow

We assume that a certain amount of kinetic energy is induced in each free particle that experienced the Λ_s-sign switch transition event. Considering the RW metric,

$$
ds^2 = -dt^2 + a^2[d\chi^2 + \chi^2(d\theta^2 + \sin^2\theta d\phi^2)], \tag{47}
$$

the physical distance is given by $r(t) = a(t)\chi$, with χ being the comoving coordinate. The geodesic equation, representing the physical radial coordinate of a free particle with a constant comoving coordinate in an RW metric, is expressed as [145]

$$
\ddot{r} - \frac{\ddot{a}}{a} r = 0. \tag{48}
$$

To elucidate the consequences of the type-II (sudden) singularity that occurs at the Λ_s-sign switch transition (see Appendix A), it is imperative to evaluate the integral of Eq. (48) over an interval surrounding the transition moment. Consider, in particular, the time interval t given by $t \in [t_{\dagger} - \varepsilon, t_{\dagger} + \varepsilon]$, where ε is a positive infinitesimal. Proceeding with this approach and given that $r = a\chi$,

$$
\int_{t_{\dagger}-\varepsilon}^{t_{\dagger}+\varepsilon} dt\,\ddot{r} - \int_{t_{\dagger}-\varepsilon}^{t_{\dagger}+\varepsilon} dt\,\frac{\ddot{a}}{a} r = 0 \Rightarrow \dot{r}|_{t_{\dagger}-\varepsilon}^{t_{\dagger}+\varepsilon} = (Hr)|_{t_{\dagger}-\varepsilon}^{t_{\dagger}+\varepsilon}. \tag{49}
$$

Consider the velocity difference[8] around the moment of singularity $t_{\dagger}$:

$$
\delta V \equiv \dot{r}^{(+)} - \dot{r}^{(-)} = H^{(+)} r(t_{\dagger}) - H^{(-)} r(t_{\dagger}). \tag{50}
$$

Given the continuity of the physical distance $r(t)$, we derive the velocity impulse as

$$
\delta V = \delta H r_{\dagger}. \tag{51}
$$

Here we denote the discontinuous increase in the Hubble parameter resulting from the sign switch of the cosmological constant, as derived from the Friedmann equation:

$$
\delta H \equiv H^{(+)} - H^{(-)}
$$
$$
= \sqrt{\frac{8\pi G \tilde{\rho}_{m0}}{3}} \Big[(a_{\dagger}^{-3} + \omega_s + \xi_s a_{\dagger}^{-2})^{\frac{1}{2}}
$$
$$
- (a_{\dagger}^{-3} - \omega_s + \xi_s a_{\dagger}^{-2})^{\frac{1}{2}} \Big]. \tag{52}
$$

The solution to the geodesic equation for a free particle, as denoted in Eq. (48), within the Λ_sCDM framework can be derived using joint boundary conditions at the transition moment, i.e., $r(t)$ is continuous at $t_{\dagger}$ and also Eq. (51). These conditions include the continuity of $r(t)$ at $t_{\dagger}$ and the

---

[8]Throughout the text, we define the left and right limits of a function as $f^{(-)} \equiv \lim_{\varepsilon \to 0} f(t_{\dagger} - \varepsilon)$ and $f^{(+)} \equiv \lim_{\varepsilon \to 0} f(t_{\dagger} + \varepsilon)$, respectively.
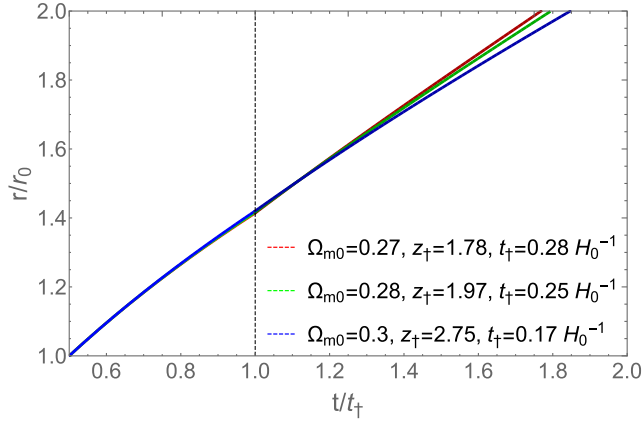
FIG. 1. Utilizing the joint boundary conditions at the transition moment $t/t_\dagger = 1$, an analytical solution to the geodesic equation for a free particle within the Λ_sCDM cosmological framework is derived. The solution is for the geodesic (C8), which maintains the continuity of the physical distance $r(t)$ and incorporates the velocity kick (51). The initial conditions $r(t/t_\dagger = 0.5) = r_0$ and $\dot{r}(t/t_\dagger = 0.5) = r_0/t_\dagger$ are imposed. We observe that the effect of the kick (at $t/t_\dagger = 1$) is insignificant. Additionally, as $(z_\dagger)$ decreases, the velocity kick intensifies, causing the ratio $\left(\frac{r}{r_0}\right)$ to reach higher values.

conditions described in Eq. (51), which account for the velocity kick. With a specified set of initial conditions for r and $\dot{r}$, we are able to derive the analytical solution (C8) (Fig. 1). Considering that the physical distance $r = a\chi$ [where $a(t)$ is the scale factor, as shown in Eq. (C6)], this follows the exact same form as $a(t)$, assuming a constant χ (see Appendix C for a detailed derivation of the scale factor in the Λ_sCDM model).

3. Effect of the type-II singularity:
Spherical collapse model

A free particle in constant comoving coordinates will infall due to the contraction of the spherical overdensity entrained by the spacetime geometry. Following the same reasoning as in Sec. III B 2, we introduce the corresponding velocity kick to a particle in the spherical overdensity as

$$\Delta V \equiv \dot{R}_{\mathrm{p},\dagger}^{(+)} - \dot{R}_{\mathrm{p},\dagger}^{(-)}, \tag{53}$$

where $\dot{R}_{\mathrm{p}} \equiv \chi_0 a H \frac{dR}{da}$. During the collapsing phase, we implement the negative branch of Eq. (36) in Eq. (53), which results in

$$\Delta V = -\chi_0 a_\dagger \left(H^{(+)} \sqrt{\frac{a_\dagger}{R_\dagger} \frac{1 + \omega_s R_\dagger^3 - \kappa_s R_\dagger}{1 + \omega_s a_\dagger^3 + \xi_s a_\dagger}} \right.$$
$$\left. - H^{(-)} \sqrt{\frac{a_\dagger}{R_\dagger} \frac{1 - \omega_s R_\dagger^3 - \kappa_s R_\dagger}{1 - \omega_s a_\dagger^3 + \xi_s a_\dagger}} \right). \tag{54}$$

4. Effect of the type-II singularity:
Modified virialization condition

We assume the transition occurs during the collapse of the overdensity (where $a_\dagger > a_{\mathrm{ta}}$) at the turnaround moment,

$$\frac{\rho_{\Lambda_s}(a_{\mathrm{ta}})}{\rho_{\mathrm{m}}(a_{\mathrm{ta}})} = \mathrm{sgn}(1/a_\dagger - 1/a_{\mathrm{ta}})e_{\Lambda_s} = -e_{\Lambda_s}, \tag{55}$$

and the potential energy of the system, at the moment when the scale factor attains the value a_{ta} and the cosmological constant is negative, is substituted according to Eq. (22) as

$$\mathcal{U}_{\mathrm{halo}} = -\frac{3}{5} \frac{GM^2}{R_{\mathrm{p}}} \left[1 - e_{\Lambda_s} \left(\frac{R_{\mathrm{p}}}{R_{\mathrm{p,ta}}} \right)^3 \right]. \tag{56}$$

Energy conservation is upheld right until the brink of the singularity's emergence at $a = a_\dagger$. If $\varepsilon > 0$ is an infinitesimally small positive quantity and $t_\dagger - \varepsilon$ represents the moment just before the singularity, then, given the continuity of R_{p}, when $\varepsilon \to 0$ we obtain

$$\mathcal{K}^{(-)} = \mathcal{U}_{\mathrm{halo}}|_{R_{\mathrm{p,ta}}} - \mathcal{U}_{\mathrm{halo}}|_{R_{\mathrm{p},\dagger}}. \tag{57}$$

Immediately after, energy conservation continues to be valid but incorporates an energy impulse attributed to the singularity. Specifically, the velocity V of a spherically symmetric shell is given by $V = \frac{\dot{R}}{R} R_{\mathrm{p}}$. This implies that for $t_\dagger + \varepsilon$, due to a velocity kick, V transitions to $V + \Delta V$ [Eq. (54)]. Consequently, this impulse affects the kinetic energy in the following manner:

$$\mathcal{K}^{(+)} = \mathcal{K}^{(-)}[1 + \Delta]^2, \tag{58}$$

where we have defined Δ as

$$\Delta \equiv \frac{\Delta V}{|V^{(-)}|} = \frac{\Delta V}{|\chi_0 a_\dagger H^{(-)} \frac{dR^{(-)}}{da}|}$$
$$= 1 - \frac{H^{(+)}}{H^{(-)}} \sqrt{\frac{(1 + \omega_s R_\dagger^3 - \kappa_s R_\dagger)(1 - \omega_s a_\dagger^3 + \xi_s a_\dagger)}{(1 + \omega_s a_\dagger^3 + \xi_s a_\dagger)(1 - \omega_s R_\dagger^3 - \kappa_s R_\dagger)}}. \tag{59}$$

From immediately post-singularity up to the point of virialization, the conservation of energy, along with the virial theorem, gives

$$\frac{R_{\mathrm{p}}}{2} \frac{d\mathcal{U}_{\mathrm{halo}}}{dR_{\mathrm{p}}} \bigg|_{R_{\mathrm{p,vir}}} + \mathcal{U}_{\mathrm{halo}}|_{R_{\mathrm{p,vir}}} = \mathcal{K}^{(+)} + \mathcal{U}_{\mathrm{halo}}|_{R_{\mathrm{p},\dagger}}. \tag{60}$$

Equations (58) and (57) combined imply the following modified *virialization condition*:

$$\frac{R_{p,vir}}{2} \frac{dU_{halo}}{dR_p}\bigg|_{R_{p,vir}} + U_{halo}\big|_{R_{p,vir}}$$

$$= (U_{halo}|_{R_{p,ta}} - U_{halo}|_{R_{p,\dagger}})(1+\Delta)^2 + U_{halo}\big|_{R_{p,\dagger}}. \quad (61)$$

Implementing the potential energy, given by Eq. (56), into Eq. (61) and taking into account that the singularity takes place subsequent to the turnaround moment, i.e., $a_\dagger > a_{ta}$, we derive

$$-\frac{1 - y_{vir}^{-3(1+w)}\Theta\eta^3}{10R_{p,vir}} + \frac{1 - y_\dagger^{-3(1+w)}\Theta u_\dagger^3}{5R_{p,\dagger}} + \frac{3\Theta y_{vir}^{-3(1+w)}R_{p,vir}^2}{10R_{ta}^3}$$

$$- (1+\Delta)^2\left(-\frac{1-\Theta}{5R_{ta}} + \frac{1 - y_\dagger^{-3(1+w)}\Theta u_\dagger^3}{5R_{p,\dagger}}\right) = 0. \quad (62)$$

Subsequently, for a cosmological constant ($w_\Lambda = -1$), Eq. (62) implies that

$$\Delta_0(-1+u_\dagger) + u_\dagger\left(1 - \frac{1}{2\eta}\right)$$

$$+ u_\dagger e_{\Lambda_s}[-1 + 2\eta^2 + \Delta_0(-1+u_\dagger^2)] = 0, \quad (63)$$

where we have defined the following dimensionless parameters:

$$\Delta_0 \equiv \Delta(2+\Delta), \qquad u_\dagger \equiv \frac{R_\dagger}{R_{ta}}.$$

Note that when $\Delta = 0$, Eq. (27) is recovered, corresponding to a collapse with a negative cosmological constant. While Eq. (63) admits an analytical solution, its complexity can hinder a straightforward physical interpretation. As such, we resort to an approximate solution. At first order in Δ_0 and for values of $u_\dagger$ close to 1, we obtain

$$\eta = \frac{1}{2}\left[1 + \frac{\Delta_0(1-u_\dagger)}{u_\dagger}\right] + \frac{e_{\Lambda_s}}{4}[1 + 2\Delta_0(1-u_\dagger^2)]$$

$$- \frac{e_{\Lambda_s}^2}{8}\left[1 + \frac{7\Delta_0(1-u_\dagger)}{u_\dagger}\right] + \dots \quad (64)$$

This approximation remains valid for $|\Delta| \ll 1$. In cases where this condition is not met, it becomes necessary to resort to the analytical solutions of Eq. (63) (Fig. 2). The collapse of an overdense region and the expansion of the Universe exert opposing effects. The impact of the singularity on the overdensity is significant when $y_\dagger \simeq 1$ and becomes smaller for values that are further away, as well as for larger values of z_{ta}, as shown in Fig. 3. Although the sudden singularity extracts kinetic energy (i.e., when $-1 \le \Delta < 0$) from the collapsing overdensity, it is notable that near the turnaround moment the velocity of the contracting overdensity approaches zero. Consequently, the "velocity brake" (occurring when $\Delta < -1$) is sufficient to reverse the direction, effectively inducing a velocity kick. This kick expands the shell once more to a slightly larger
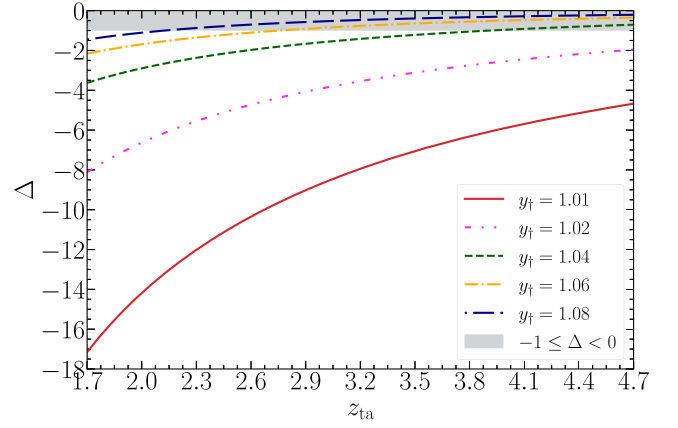

FIG. 2. Variation of Δ with respect to z_{ta}, obtained by keeping $y_\dagger \in [1.01, 1.02, 1.04, 1.06, 1.08]$ constant. The collapse of the overdense region and the expansion of the Universe exert opposing effects. Consequently, the emergence of the sudden singularity effectively dissipates kinetic energy ($\Delta < 0$), as demonstrated above. The shaded gray area represents the region of $-1 \le \Delta < 0$, where only the kinetic energy is extracted from the overdensity. Meanwhile, for $\Delta < -1$, the overdensity expands once more to a slightly larger value of a new physical radius, before it collapses again and eventually virializes.

value of a new physical radius, before it collapses again and eventually virializes.

Additionally, we can assume a brief period of time after the turnaround but before the shell crossing where we can still apply the negative branch of Eq. (36). Thus, by integrating Eq. (36) throughout the period where the scale factor ranges from a_{ta} to $a_\dagger$, we obtain the following equation:

$$\int_{u_\dagger}^1 du \sqrt{\frac{u}{a_{ta}^{-3}(1+\delta_{ta})(1-u) + \omega_s u(1-u^2)}}$$

$$= \int_1^{y_\dagger} dy \sqrt{\frac{y}{a_{ta}^{-3} - \omega_s y^3 + \xi_s a_{ta}^{-2}y}}. \quad (65)$$

We evaluate $u_\dagger$ using Eq. (65) and then incorporate η, as calculated in Eq. (64).

Subsequently, the value of R_{vir} is ascertained in accordance with Eq. (69), leading to the determination of the anticipated ratios, as discussed in Sec. III C.

Assuming that $t_{vir} \simeq 2t_{ta}$ and that the collapse is completed when $t = t_{vir}$, Eq. (34) yields ($y_\dagger > 1$)

$$\int_0^{y_\dagger} dy \sqrt{\frac{y}{a_{ta}^{-3} - \omega_s y^3 + \xi_s a_{ta}^{-2}y}}$$

$$+ \int_{y_\dagger}^{y_{vir}} dy \sqrt{\frac{y}{a_{ta}^{-3} + \omega_s y^3 + \xi_s a_{ta}^{-2}y}}$$

$$= 2\int_0^1 dy \sqrt{\frac{y}{a_{ta}^{-3} - \omega_s y^3 + \xi_s a_{ta}^{-2}y}}, \quad (66)$$
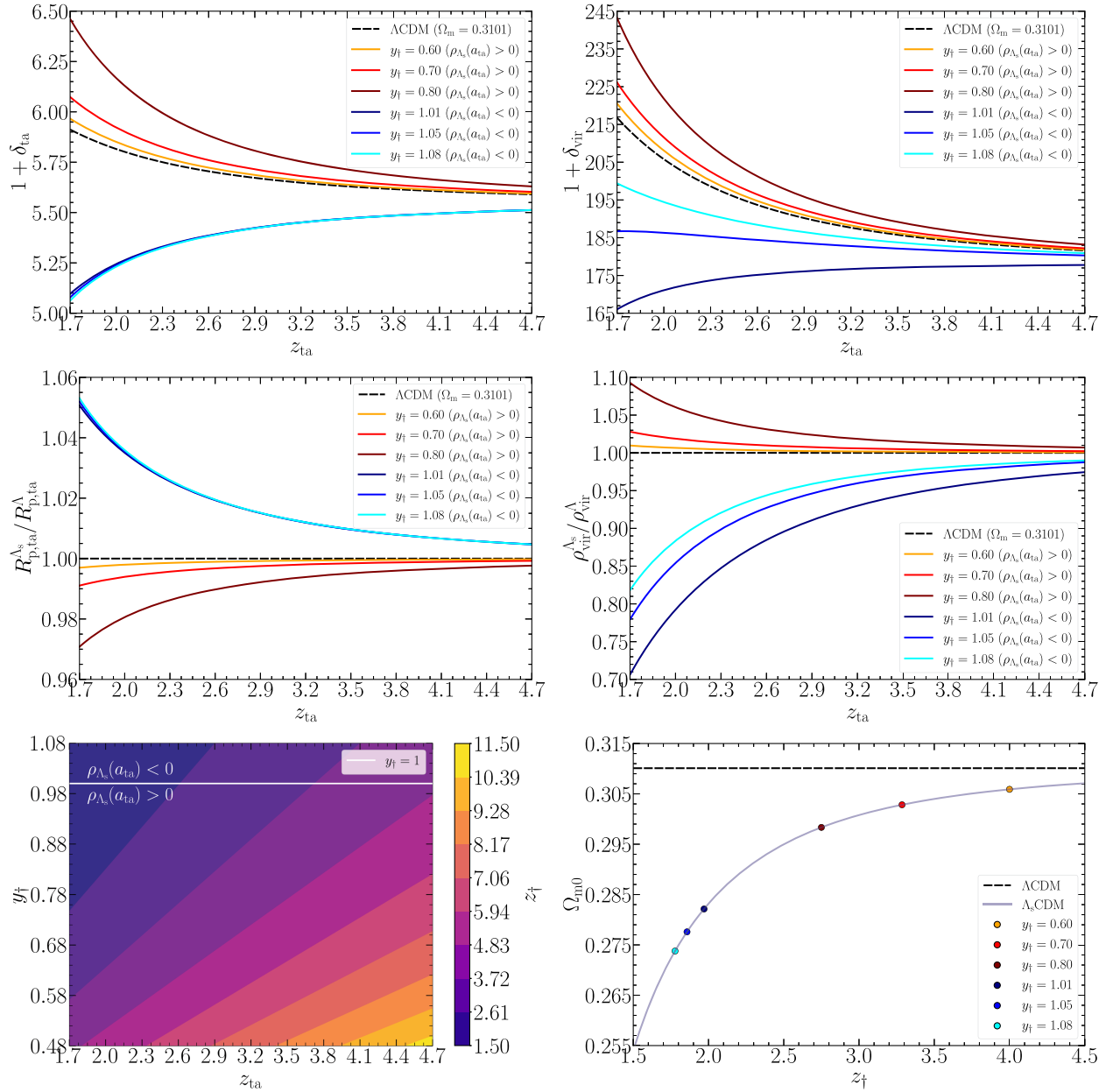
FIG. 3. Numerical analysis performed to calculate δ_{ta}, δ_{vir}, ρ_{vir}, and $R_{\mathrm{p,ta}}$ for post-turnaround (shades of blue) and pre-turnaround (shades of red) cases, where the cosmological parameters are derived from the analysis given in Appendix D. Each panel is obtained by varying $1.7 \leq z_{\mathrm{ta}} \leq 4.7$ for constant $y_{\dagger} \equiv a_{\dagger}/a_{\mathrm{ta}}$. The corresponding $z_{\dagger}$ value for a given z_{ta} can be calculated via $1 + z_{\dagger} = (1 + z_{\mathrm{ta}})/y_{\dagger}$. Even though we use the same physical matter density parameter throughout the analysis, the Ω_{m0} parameters will be different for both models. For a given $z_{\dagger}$, one can easily find the corresponding Ω_{m0} for the Λ_{s}CDM model [see Eq. (D7)]. For the upper left, upper right, and middle right figures, curves for $(y_{\dagger} < 1)$ appear above the dashed line (ΛCDM), with density/overdensity increasing as $(y_{\dagger})$ values rise. For $(y_{\dagger} > 1)$, despite a similar increase, curves remain below the dashed line. An exception is the upper left figure, where for $(y_{\dagger} > 1)$, overdensity decreases as $(y_{\dagger})$ increases. In the middle left figure, curves for $(y_{\dagger} = 0.6, 0.7, 0.8)$ are below the dashed line, decreasing sequentially, while those for $(y_{\dagger} = 1.08, 1.05, 1.01)$ are above but also decrease sequentially. The lower right figure shows that the highest point corresponds to $(y_{\dagger} = 0.6)$, with subsequent values following in a labeled sequence.

from which we obtain

$$
\int_1^{y_\dagger} dy \sqrt{\frac{y}{a_{\mathrm{ta}}^{-3} - \omega_s y^3 + \xi_s a_{\mathrm{ta}}^{-2} y}}
$$
$$
+ \int_{y_\dagger}^{y_{\mathrm{vir}}} dy \sqrt{\frac{y}{a_{\mathrm{ta}}^{-3} + \omega_s y^3 + \xi_s a_{\mathrm{ta}}^{-2} y}}
$$
$$
= \int_0^1 dy \sqrt{\frac{y}{a_{\mathrm{ta}}^{-3} - \omega_s y^3 + \xi_s a_{\mathrm{ta}}^{-2} y}}. \tag{67}
$$

It then becomes feasible to deduce the value of a_{vir} in terms of a_{ta} through Eq. (32) and subsequently δ_{vir} from Eq. (33).

C. Contrasting Λ_sCDM with standard ΛCDM: Insights into the physical outcomes

Based on Eqs. (11) and (20), the physical radius of the overdensity at turnaround is expressed as

$$
R_{\mathrm{p,ta}} = \left[\frac{3M}{4\pi(1 + \delta_{\mathrm{ta}})\tilde{\rho}_{\mathrm{m0}}} \right]^{\frac{1}{3}} a_{\mathrm{ta}}. \tag{68}
$$

Furthermore, using the definition of η from Eq. (28), we can write the virialized physical radius of the overdensity as

$$
R_{\mathrm{p,vir}} = (1 + z_{\mathrm{ta}})^{-1} \left[\frac{3M}{4\pi(1 + \delta_{\mathrm{ta}})\tilde{\rho}_{\mathrm{m0}}} \right]^{\frac{1}{3}} \eta. \tag{69}
$$

Consequently, the ratio of the virialized matter density in the Λ_sCDM model to that in the ΛCDM model [1,4] reads

$$
\frac{(\rho_{\mathrm{vir}})_{\Lambda_s}}{(\rho_{\mathrm{vir}})_\Lambda} \equiv \left[\frac{(R_{\mathrm{p,vir}})_{\Lambda_s}}{(R_{\mathrm{p,vir}})_\Lambda} \right]^{-3} = \frac{(1 + \delta_{\mathrm{ta}}^{\Lambda_s})}{(1 + \delta_{\mathrm{ta}}^\Lambda)} \left[\frac{\eta(e_{\Lambda_s})}{\eta(e_\Lambda)} \right]^{-3}. \tag{70}
$$

The physical effects of the Λ_s-sign switch (AdS-dS) transition can primarily be understood by considering the timing of the transition relative to the turnaround moment, distinguishing between the pre-turnaround ($z_\dagger > z_{\mathrm{ta}}$) and post-turnaround ($z_{\mathrm{ta}} < z_\dagger$) Λ_s-sign switch transitions. These effects are demonstrated in Fig. 3 where, for a realistic assessment, the cosmological parameters for both models, namely, Λ_sCDM (for various $z_\dagger$ cases) and ΛCDM, are chosen to ensure consistency with the *Planck*-CMB power spectra, as detailed in Appendix D.

1. Pre-turnaround Λ_s-sign switch transition ($z_\dagger > z_{\mathbf{ta}}$)

We first consider the case $y_\dagger < 1$, where the Λ_s-sign switch transition occurs before the turnaround, i.e., $z_\dagger > z_{\mathrm{ta}}$. Our findings indicate that if this transition happens before turnaround, the density contrast at turnaround (δ_{ta}) will be higher than in the ΛCDM model, as shown in the top-left panel of Fig. 3. The rationale behind this is as follows. Because the transition has already occurred, the positive cosmological constant has already begun to influence the curvature of the halo as described by Eq. (15) ($\omega_s > 0$). On the other hand, as illustrated in Fig. 4 which is plotted by choosing $z_{\mathrm{ta}} = 2$ (noting that different values of z_{ta} do not
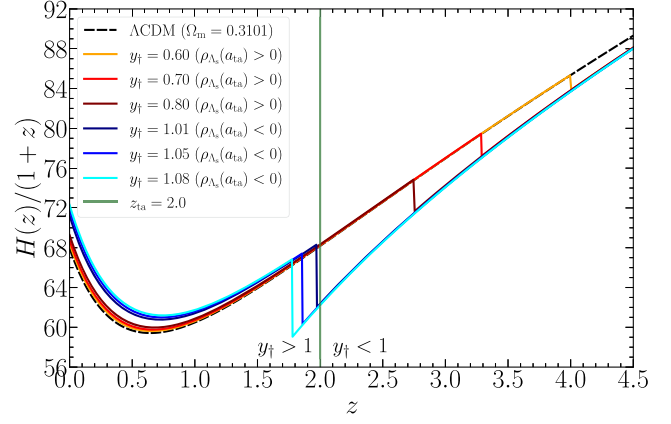

FIG. 4. $\dot{a} \equiv H(z)/(1 + z)$ vs z plotted for constant $y_\dagger \equiv a_\dagger/a_{\mathrm{ta}}$, by fixing the turnaround redshift at 2 (i.e., $z_{\mathrm{ta}} = 2$). We have applied the method described in Appendix D to determine the cosmological parameters. For a fixed a_{ta}, as $y_\dagger \to 0$, the scale factor of the transition approaches $a_\dagger \to 0$ and the Λ_sCDM model dynamics becomes similar to ΛCDM. Meanwhile, as $y_\dagger \to 1/a_{\mathrm{ta}}$, the transition approaches today. Also note that before the transition the expansion rate of the Universe is smaller ($\dot{a}^{\Lambda_s\mathrm{CDM}} < \dot{a}^{\Lambda\mathrm{CDM}}$), but after the transition it is faster ($\dot{a}^{\Lambda_s\mathrm{CDM}} > \dot{a}^{\Lambda\mathrm{CDM}}$) than the ΛCDM universe. As ($y_\dagger$) increases, the transition occurs at lower redshifts.

change the trends in the plots), a larger $y_\dagger < 1$ results in the overdensity evolving under the negative cosmological constant's influence for a longer period. This implies that for larger $y_\dagger < 1$ values the negative cosmological constant's slowing-down effect on the overdensity's expansion, due to its induced gravitational attraction, lasts longer, leading to denser structures. Consequently, we observe generally higher δ_{ta} values for the Λ_sCDM model compared to the ΛCDM model in the top-left panel of Fig. 3, with this difference increasing for larger $y_\dagger$ values, as long as $y_\dagger < 1$. We note that the expansion rate of the background Universe, $\dot{a} = \frac{H(z)}{1+z}$, around z_{ta} is almost identical across various $y_\dagger$ values for a given z_{ta}, as seen in Fig. 4 which is plotted by choosing $z_{\mathrm{ta}} = 2$ as an example. Thus, the expansion rate of the Universe at or around the turnaround moment does not intervene in and influence our discussions on the value of δ_{ta} within the Λ_sCDM framework. And, of course, since δ_{ta} and $R_{\mathrm{p,ta}}$ are interrelated through Eq. (68), a higher δ_{ta} corresponds to a smaller $R_{\mathrm{p,ta}}$ and vice versa for a given value of z_{ta} or a_{ta}. Finally, the collapsing phase of the overdensity proceeds under the influence of a positive cosmological constant until virialization, similar to the standard ΛCDM model. Therefore, evidently, the larger values of δ_{ta} achieved in the Λ_sCDM model compared to the ΛCDM model give rise to corresponding larger values of δ_{vir} and $\rho_{\mathrm{vir}}^{\Lambda_s}$, as seen in the top- and middle-right panels of Fig. 3, respectively.

2. Post-turnaround Λ_s-sign switch transition ($z_{\mathbf{ta}} > z_\dagger$)

We now consider the case $y_\dagger > 1$, where the Λ_s-sign switch transition occurs after the turnaround, i.e., $z_{\mathrm{ta}} > z_\dagger$,

focusing on the phase during which the halo is collapsing, but well before shell crossing, when the halo is still homogeneous and isotropic. In this phase, the density contrast at the turnaround, δ_ta, will be lower compared to that in the ΛCDM model, with this effect being more pronounced at lower values of z_ta, as seen in the top-left panel of Fig. 3. The rationale behind this is as follows. In the ΛCDM model, the overdensity experiences a positive cosmological constant throughout its evolution. In contrast, in the post-turnaround Λ_s-sign switch transition case of the Λ_sCDM model the overdensity experiences a negative cosmological constant until and for some time after reaching the turnaround radius. This implies that less matter energy density is required for the overdensity to achieve turnaround due to the enhancing gravitational attraction effects of the negative cosmological constant (in contrast to the positive cosmological constant), leading to less curvature for the overdensity. We note that the lower the z_ta, the larger difference in δ_ta between the Λ_sCDM and ΛCDM models. This is understandable as at lower redshifts the cosmological constant is more dominant in both models, but it is negative in the Λ_sCDM and positive in the ΛCDM model. Specifically, the lower the z_ta, the higher the δ_ta in the ΛCDM model, while the lower the z_ta, the lower the δ_ta in the Λ_sCDM model.

Note that δ_ta is almost identical for a given z_ta value, with only barely visible differences at lower z_ta values for various $y_\dagger$ values. This is explained by the fact that for $z > z_\text{ta}$ the expansion rates of the Universe for different $y_\dagger$ values are almost the same, allowing the overdensities to evolve through nearly identical background Universe dynamics until turnaround is achieved, as seen in Fig. 4 which is plotted by choosing $z_\text{ta} = 2$ as an example. Note that for different $y_\dagger > 1$ values, we use the same physical matter density value and fix the angular size of the sound horizon at the last-scattering surface to ensure consistency with CMB-*Planck* spectra (see Appendix D), resulting in slightly different values for Ω_m0, corresponding to slightly different H_0 values. This implies, for a given z_ta, slightly different matter density parameters/expansion rates of the Universe at the times when the overdensity is evolving towards the turnaround, and the time taken to reach the turnaround radius would be slightly different. The Ω_m0 can be read from the bottom panels of Fig. 3; for the $y_\dagger = \{1.01, 1.05, 1.08\}$ values we used, we have $z_\dagger = \{1.97, 1.86, 1.78\}$ and $\Omega_\text{m0} = \{0.2821, 0.2777, 0.2739\}$. In other words, $\dot{a}$ is almost identical across all Λ_sCDM cases for $y_\dagger > 1$ for $z > z_\text{ta}$ and thus is not expected to cause significant variations in δ_ta for different $y_\dagger > 1$ values. In these cases, the overdensity experiences the negative cosmological constant for a nearly identical duration; see Fig. 4. The minor variations in δ_ta are attributed to slightly different values of Ω_m0, implying slightly different expansion rates of the Universe and hence a slightly different passage of time taken until turnaround is achieved. In the middle-left panel

of Fig. 4, we plot the ratio of the physical radius of the halo at the turnaround in the Λ_sCDM model to that in the ΛCDM model, viz., $R_\text{p,ta}^{\Lambda_\text{s}}/R_\text{p,ta}^{\Lambda}$.[9] We observe that $R_\text{p,ta}^{\Lambda_\text{s}}/R_\text{p,ta}^{\Lambda} > 1$, being larger for lower values of z_ta, and it is almost identical for different $y_\dagger > 1$ values with a barely visible difference for small z_ta values. This aligns with expectations when considering Eq. (15) for $\omega \to -\omega_\text{s}$, implying the higher values of $R_\text{p,ta}$ correspond to lower values of δ_ta.

Finally, in the top-right panel of Fig. 3 we plot the density contrast at the moment of virialization, δ_vir, for the cases where the Λ_s-sign switch transition occurs during the collapsing phase, before the halo virializes. It is conceivable that the δ_vir values in the Λ_sCDM are lower than in the ΛCDM model, similar to the situation with δ_ta. However, we immediately see that, although this expectation holds, unlike with the situation for δ_ta, the δ_vir values differ significantly for different $y_\dagger$ values and become more pronounced for lower z_ta values. This phenomenon is not surprising and can roughly be explained as follows. As seen in Fig. 4 (plotted by choosing $z_\text{ta} = 2$ as an example), the larger the value of $y_\dagger$, the greater the difference between $z_\dagger$ and z_ta, implying that the Λ_s-sign switch transition occurs later in the collapsing phase of the overdensity for larger $y_\dagger > 1$ values. That is, given that δ_ta is almost the same for a given z_ta for different values of $y_\dagger$, for larger $y_\dagger$ values, the Λ_s-sign switch transition occurs when the overdensity is more compact, and thereby it is conceivable that the rapid increase in the Universe's expansion rate at the transition will have less influence on the collapsing overdensity for larger $y_\dagger > 1$ values. A more precise, but also more concise, explanation is as follows. We observe that the impact of the singularity at $z_\dagger$ on the overdensity is considerable when $y_\dagger \simeq 1$ and diminishes for values further from 1 or for larger z_ta values. The singularity extracts kinetic energy (i.e., when $-1 \leq \Delta < 0$), leading to a "velocity brake" in the collapse. Conversely, when $\Delta < -1$, it induces a velocity kick, reversing the direction of the collapse and reexpanding the shell to a slightly larger new physical radius before its eventual collapse and virialization. This effect, observable in Fig. 2, suggests that higher Δ values result in lower virialized densities in the halo.

IV. IMPACT OF BACKGROUND EXPANSION ON BOUND SYSTEMS

A. Newtonian approximation of a bound system in an expanding background

Numerous studies have been devoted to exploring the impacts of cosmic expansion on bound systems [146,148,156–160]. In the Newtonian limit, the vicinity of a point mass M situated within a dynamically expanding background is characterized as follows:

---

[9]The results are independent of the halo's mass, as demonstrated in Eq. (68).

$$ds^2 = -\left(1 - \frac{2GM}{a\chi}\right)dt^2 + a^2[d\chi^2 + \chi^2(d\theta^2 + \sin^2\theta d\phi^2)],$$

$$(71)$$

where t is the comoving time and $a \equiv a(t)$. Interpreting the gravitational field of the point mass as a *weak field*, and by admitting *low velocities*, the geodesic equations can be differentiated with respect to the coordinate time t as

$$\ddot{x}^\mu + \Gamma^\mu_{\nu\sigma}\dot{x}^\nu\dot{x}^\sigma = 0, \tag{72}$$

where $\dot{} \equiv d/dt$. For the geodesic equation in the χ coordinate, considering $\theta = \pi/2$ in the equatorial plane, we derive

$$\frac{GM}{\chi(t)^2 a(t)^3} - \chi(t)\dot{\phi}(t)^2 + \frac{2\dot{a}(t)\dot{\chi}(t)}{a(t)} + \ddot{\chi}(t) = 0. \tag{73}$$

Similarly, the geodesic equation for x^3, taking $\theta = \pi/2$ again, yields

$$\frac{2\dot{a}(t)\dot{\phi}(t)}{a(t)} + \frac{2\dot{\phi}(t)\dot{\chi}(t)}{\chi} + \ddot{\phi}(t) = 0 \Rightarrow \frac{d}{dt}[(a\chi)^2\dot{\phi}] = 0. \tag{74}$$

Defining $L = (a\chi)^2\dot{\phi}$ as the angular momentum per unit mass, we express the geodesic equation from Eq. (73) in terms of the physical radial coordinate $r = a\chi$ as follows:

$$\ddot{r} - \frac{\ddot{a}}{a}r - \frac{L^2}{r^3} + \frac{GM}{r^2} = 0. \tag{75}$$

Considering a moment in time t_0 where expansion can be disregarded [i.e., $\dot{r}(t_0) = 0$], we define the physical radius of an orbit as $r_0 \equiv r(t_0)$. The angular speed at this moment, neglecting expansion, is described as

$$\dot{\phi}^2|_{t=t_0} = \frac{L^2}{r_0^4} \equiv \omega_0^2 \equiv \frac{GM}{r_0^3}. \tag{76}$$

Given the condition outlined in Eq. (76), this leads to the conclusion that $L^2 = GMr_0$. While a circular orbit with a constant physical radius does not exist at all times, r_0 represents the radius at a specific instant. Under the condition that the initial angular speed is significant enough to overlook cosmic expansion, it approximates a stable Newtonian circular orbit, assuming $L^2 \neq 0$ and $\dot{r} = 0$ at all times.

Additionally, considering a rescaling $d/dt = t_{\text{init}}^{-1}d/d\bar{t}$ and $' \equiv d/d\bar{t}$ (where t_{init} is the initial cosmic time selected for the system), we derive from Eq. (75)

$$\bar{r}'' = \frac{\bar{\omega}_0^2}{\bar{r}^3} - \frac{\bar{\omega}_0^2}{\bar{r}^2} + \frac{a''}{a}\bar{r}, \tag{77}$$

where

$$\frac{a''}{a} = -\frac{1}{2}(H_0 t_{\text{init}})^2\Omega_{\text{m0}}\left[a^{-3} - 2\omega_s a^{-1}\delta(1/a_\dagger - 1/a)\right. $$
$$\left. - 2\omega_s\text{sgn}(1/a_\dagger - 1/a)\right], \tag{78}$$

and

$$\bar{r} \equiv \frac{r}{r_0}, \quad \bar{\omega}_0 \equiv \omega_0 t_{\text{init}}, \quad \bar{t} \equiv \frac{t}{t_{\text{init}}}, \quad \dot{\phi} \equiv \frac{\bar{\omega}_0}{\bar{r}^2}. \tag{79}$$

The final step before proceeding to solve Eq. (77) involves initiating from an orbit with a rescaled radius, $\bar{r}(t_{\text{init}}) = s$, taking into account the expanding background. This is achieved by setting the rhs of Eq. (77) to zero and solving for s:

$$\bar{\omega}_0^2(1 - s) + \left.\frac{a''}{a}\right|_{t_{\text{init}}} s^4 = 0. \tag{80}$$

Subsequently, we numerically solve the geodesic equation, as presented in Eq. (77), for a bound system. Numerical examples of bound orbits within the Λ_sCDM mode are demonstrated in Figs. 5 and 5.

B. Physical outcomes

We consider a point particle with a path parametrized by the proper time τ. In this setting, the x^0-geodesic equation is

$$\frac{d}{d\tau}\left[\frac{dt}{d\tau}\left(1 - \frac{2GM}{a\chi}\right)\right] = -H(a\chi)\frac{dt}{d\tau}\left[\frac{L^2}{(a\chi)^3} + \frac{1}{a\chi}\left(a\frac{d\chi}{d\tau}\right)^2\right]. \tag{81}$$

For the first integral of a timelike geodesic, described by $ds^2 = -d\tau^2$ and assuming $\theta = \pi/2$, we redefine the metric from Eq. (71) as

$$-1 = -\left(1 - \frac{2GM}{a\chi}\right)\left(\frac{dt}{d\tau}\right)^2 + a^2\left(\frac{d\chi}{d\tau}\right)^2 + \frac{L^2}{(a\chi)^2}. \tag{82}$$

Assuming a sufficiently small time interval where every cosmic bound system maintains a physical radius $r = a\chi$

TABLE I. Clusters of galaxies form massive, virialized structures. Nevertheless, this is not the case for superclusters. Assuming an initial angular speed defined by $\omega_0^2 = GM/r_0^3$, we derive some very rough typical scales for both galaxy clusters and superclusters [161–165].

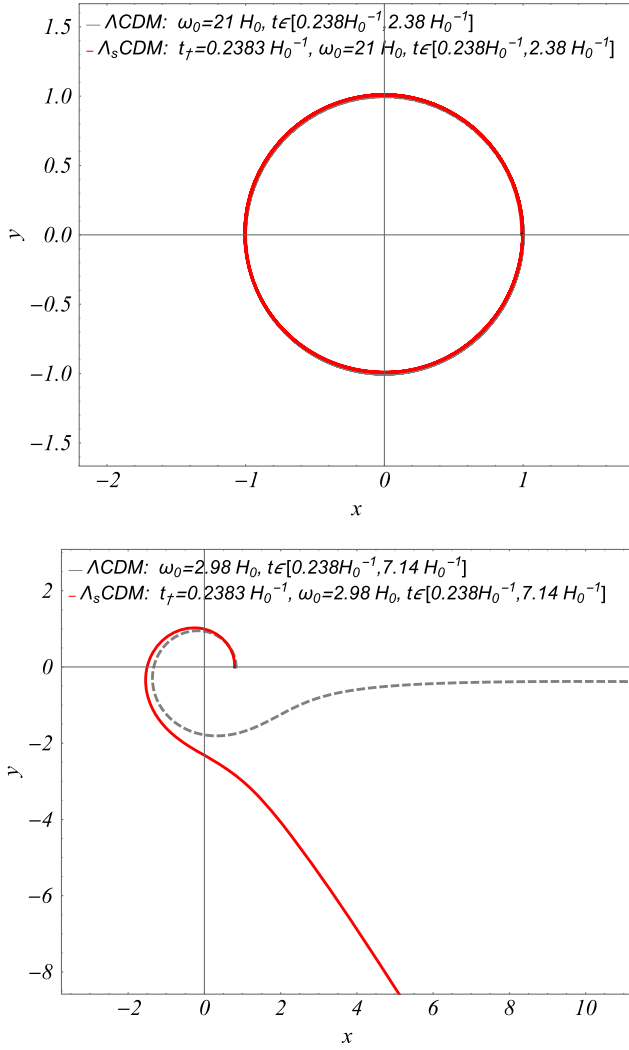| System	$M[M_\odot]$	R[Mpc]	$T_0[H_0^{-1}]$	$\omega_0[H_0]$
Cluster	$\sim10^{15}$	~2	~1	~10
Supercluster	$\sim10^{16}$	~100	~100	~0.01

FIG. 5. A particle in orbit, embedded in ΛCDM (gray) and Λ_sCDM (red), with $t_\dagger = 0.2383 H_0^{-1}$ for $\Omega_{m0} = 0.29$, and $t_{\text{init}} = 0.238 H_0^{-1}$. The initial angular velocity is set as $\omega_0 = 21 H_0$ (top) and $\omega_0 = 2.98 H_0$ (bottom) (see also Table I). We initiate a circular orbit against an expanding background, i.e., with a rescaled radius $\bar{r}(t_{\text{init}}) = s$ and $\dot{r}(t_{\text{init}}) = 0$. The s is determined by solving Eq. (80). Subsequently, we numerically solve Eq. (77) in each case. The black dot represents the position of the particle in orbit in the rescaled $x - y$ plane at the moment of the singularity.

and adheres to the approximation $H(a\chi) \ll 1$, a particle in orbit with this radius will conform to this approximation. If we also assume a small peculiar velocity, the second term in Eq. (81) is deemed higher order, simplifying the equation to

$$\frac{dt}{d\tau}\left(1 - \frac{2GM}{a\chi}\right) = k \equiv \text{const.} \qquad (83)$$

Upon integrating Eq. (83) into Eq. (82), we derive

$$-1 = -\left(1 + \frac{2GM}{a\chi}\right)k^2 + a^2\left(\frac{d\chi}{d\tau}\right)^2 + \frac{L^2}{(a\chi)^2}. \qquad (84)$$

In the regime of small peculiar velocities ($dt \simeq d\tau$), this results in an expression for the quasienergy:

$$E \equiv \frac{k^2 - 1}{2} = \frac{1}{2}\dot{r}^2 - \frac{GM}{r} - Hr\dot{r} + \frac{1}{2}H^2 r^2 + \frac{L^2}{2r^2}. \qquad (85)$$

Consider a particle initially moving in an orbit at $r(t_{\text{init}}) = sr_0$ [with $\dot{r}(t_{\text{init}}) = 0$] in a bound system. During a short time interval around $t_\dagger$, if the approximations $\bar{r}(t_{\text{init}}) \simeq 1$ and $\dot{\bar{r}} \simeq 0$ are valid, then Eq. (85) simplifies to

$$E = \frac{1}{2}(H + \delta H)^2 r_0^2 + \frac{(\omega_0 r_0)^2}{2} - (\omega_0 r_0)^2. \qquad (86)$$

Given these approximations, consider any particle in a system with mass M that initiates its orbit at a time t_{init}, where $t_{\text{init}} \in (t_\dagger - T, t_\dagger)$ and T is sufficiently small. The particle has an initial angular momentum L and $\dot{r}(t_{\text{init}}) = 0$. Also, the particle's initial physical radius is approximately $r(t_{\text{init}}) \simeq r_0 \simeq r(t_\dagger)$. We define the *critical angular speed*, ω_{crit}, at the moment $t_\dagger$, if and only if the total energy $E = 0$, according to the equation

$$\omega_{\text{crit}} = H + \delta H. \qquad (87)$$

Given that the singularity is relatively weak, it alone cannot dissociate any bound system before the continual expansion of the Universe does. Thus, the dissociation of bound orbits is primarily driven by cosmic expansion, with the singularity inducing a minor perturbation that slightly increases the Hubble value at a specific instant. This perturbation contributes minimally to the dissociation of a bound orbit. Notably, the timing of initiating a bound orbit significantly influences its evolution, as demonstrated in Fig. 5, where we initiate an orbit near the moment of the singularity. We calculate the critical angular speed, ω_{crit}, to be approximately 3 for Λ_sCDM and 2.9 for ΛCDM.

Given the brief period when the cosmological constant is negative in the Λ_sCDM model compared to its positive phase, variations in orbits relative to those equivalent orbits in the ΛCDM model suggest a scenario in the Λ_sCDM model where orbits with sufficiently low angular speed may dissociate, unlike their counterparts in the ΛCDM model. However, this dynamic changes when orbits are initiated far in the past, away from the singularity. In such cases, the negative cosmological constant in the Λ_sCDM model aids in maintaining the orbit's binding over a significant period, preventing the singularity from weakening the gravitational attraction enough to cause more dissociation than in the ΛCDM model.

The critical initial angular speed, ω_{crit}, approximated from Eq. (87), acts as a threshold. For bound systems with
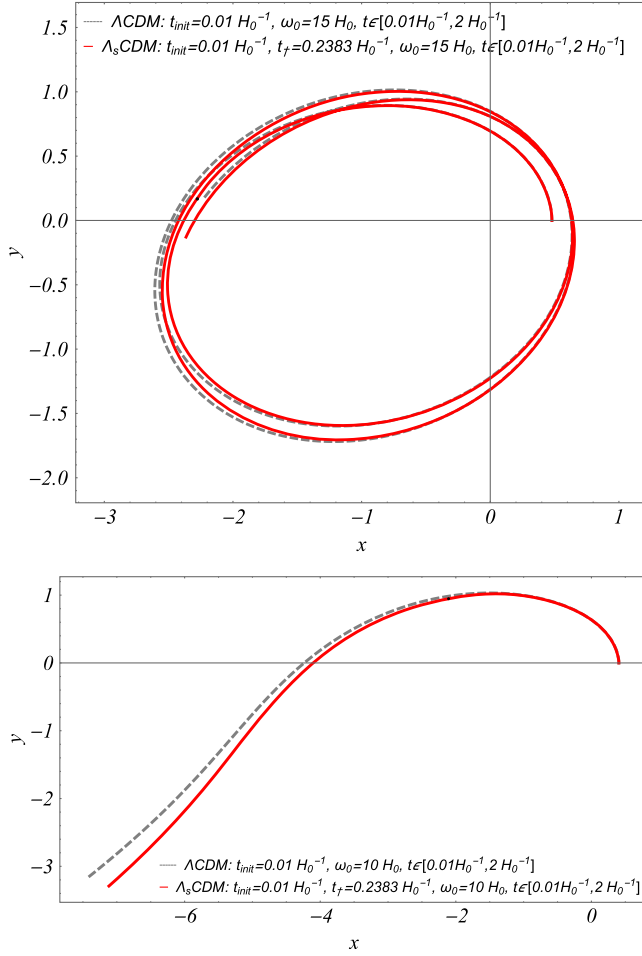
FIG. 6. A particle in orbit, embedded in ΛCDM (gray) and Λ_sCDM (red), with $t_\dagger = 0.2383 H_0^{-1}$ for $\Omega_{m0} = 0.29$ and $t_{init} = 0.01 H_0^{-1}$. The initial angular velocity is set as $\omega_0 = 15 H_0$ (top) and $\omega_0 = 10 H_0$ (bottom) (see also Table I). We initiate a circular orbit against an expanding background, i.e., with a rescaled radius $\bar{r}(t_{init}) = s$ and $\dot{r}(t_{init}) = 0$. The s is determined by solving Eq. (80). Subsequently, we numerically solve Eq. (77), in each case. The black dot represents the position of the particle in orbit in the rescaled $x - y$ plane at the moment the singularity.

an angular speed ω_0—the speed in a Newtonian bound system disregarding cosmic expansion—dissociation due to the cosmic expansion occurs if and only if $\omega_{crit} > \omega_0$. This approximation holds mainly for orbits beginning at moments near $t_\dagger$. The results from Eq. (87) align well with those obtained numerically from the geodesic equation (75), as shown in Fig. 5. However, this method does not accurately approximate numerical results for orbits starting well before the moment under study; such an example is shown in Fig. 6.

V. CONCLUSION

The Λ_sCDM model [47–50] has emerged as a highly promising approach to addressing major cosmological

tensions within the standard ΛCDM model and its canonical extensions, such as the H_0 and S_8 tensions. This achievement is realized through the introduction of a single parameter, $z_\dagger$, to the six-parameter base ΛCDM model. This parameter determines the timing of an abrupt AdS-dS transition, changing from $\Lambda_s = -\Lambda_{s0}$ for $z > z_\dagger$ to its late-time positive value $\Lambda_s = \Lambda_{s0}$ for $z < z_\dagger$. Examining the implications of adopting the Λ_sCDM model framework for the Universe's evolution, especially on the formation and evolution of bound cosmic structures, is crucial. The switch to the Λ_sCDM model is anticipated to impact bound cosmic structures for three primary reasons: (i) the negative cosmological constant (AdS) phase for $z > z_\dagger \sim 2$, (ii) the abrupt transition itself, marked by a sudden jump in the Universe's expansion rate—a type-II (sudden) singularity—at $z = z_\dagger$, and (iii) the increased expansion rate compared to the ΛCDM model for $z < z_\dagger$. Despite the faster expansion rate, the Λ_sCDM and ΛCDM models are otherwise identical for $z < z_\dagger$. All of these aspects warrant thorough investigation as their potential effects can be used to test the unique predictions of the model. In this paper, we analyzed the nonlinear evolution of a spherical overdensity within the Λ_sCDM cosmology. We began by revisiting the dynamics of spherical collapse within the ΛCDM framework and then integrated the physical effects of the AdS-dS transition into the spherical collapse model. This integration was accomplished by adjusting the Friedmann equations for the Λ_sCDM model. Furthermore, using energy considerations, we made predictions about the eventual state of the halo, dependent on the timing of the transition relative to the turnaround. Specifically:

(1) If the turnaround occurs after the transition, in what we refer to as the *pre-turnaround transition*, halos that form and undergo this transition exhibit virialized overdensities exceeding those predicted by the *Planck*-ΛCDM model, particularly at lower turnaround redshifts. This observation can be attributed to the increased δ_{ta} values resulting from a period with a negative cosmological constant, which facilitates the formation of denser structures. In both the ΛCDM and Λ_sCDM models under pre-turnaround transition scenarios, the expansion of the Universe reaches the turnaround radius with a positive cosmological constant. This results in greater curvature and matter overdensity at the turnaround radius compared to the post-turnaround case.

(2) If the turnaround occurs before the transition, in what we refer to as the *post-turnaround transition*, halos experiencing this transition typically achieve virialization at lower overdensities compared to those predicted by *Planck*-ΛCDM. This observation can be attributed to the negative cosmological constant at the turnaround, necessitating a lower matter overdensity at this moment, which results in reduced curvature at turnaround. Consequently, in

this scenario, overdensities attain a larger maximum physical radius owing to their diminished matter overdensity and curvature.

In the abrupt Λ_sCDM model, we have observed that the Hubble parameter displays a discontinuity at a specific past redshift, $z = z_\dagger$. This discontinuity leads to a type-II (sudden) singularity at $z = z_\dagger$, as discussed in Appendix A and supported by [122]. Despite its mild nature, this singularity imparts a velocity kick to particles. We have shown that smoothing out the abrupt behavior effectively eliminates this singularity, even when the transition occurs very rapidly. Hence, our findings regarding the velocity kick pertain to the extreme version of the Λ_sCDM model. However, we demonstrated that, even in this case, we ascertain that the singularity's impact on Newtonian bound virialized systems is minimal, thereby not threatening the model's viability in this context. Notably, the singularity, being relatively weak, does not lead to the dissociation of large bound systems before this is done by the Universe's continuous background expansion. For instance, large clusters or superclusters, corresponding to $\omega_0 < 10H_0$, will be dissociated by the background expansion but remain practically unaffected by the singularity (as illustrated in Figs. 5 and 6). The expansion in both the Λ_sCDM and ΛCDM models tends to induce dissociation of bound systems at scales of large clusters and above at similar levels. Therefore, the presence of unbound orbits is primarily driven by Universal expansion, with the singularity merely causing an increase in the Hubble expansion rate at a specific moment. Interestingly, the negative cosmological constant in the Λ_sCDM model tends to enhance the stability of bound systems due to its attractive gravity effects.

The outcomes of our analysis open intriguing avenues for future research. Broadening the scope, a natural extension could involve generalizing the spherical collapse model to accommodate a more diverse range of sudden cosmological singularities. Another promising direction is the investigation of the impact of the Λ-sign switch transition on gravitational waves traversing the sudden cosmological singularity, as discussed in [128]. Moreover, delving into the physical mechanisms that induce the sign switch of the cosmological constant, as explored in Refs. [113–115], remains a significant area of interest. The Λ_sCDM model, with its potential to address the Hubble and S_8 tensions, may also influence early-Universe structure growth due to its period of a negative cosmological constant. Our current study assumed a uniform transition in a homogeneous universe. However, slight inhomogeneities could lead to timing variations in this transition, as suggested in [49]. Such variations might result in different regions of the Universe experiencing the cosmological constant's sign switch at distinct redshifts, with potential implications for galaxy formation. This scenario could encompass sudden singularities of varying intensities and even halos formed entirely under a negative cosmological constant. Recent observations from the JWST hint at more intense early galaxy formation, potentially aligning with our model's implications. Although our results show only minor deviations from the ΛCDM model for structures formed at higher redshifts, they underscore the necessity for further exploration. In particular, the prospect of halos forming entirely under a negative cosmological constant could present a different narrative and warrants detailed investigation.

The *Mathematica* (v12) and PYTHON files used for the production of the figures and the derivation of the main results of the analysis can be found at the camarman/transition-dynamics-lscdm repository under the MIT license.

APPENDIX A: DEMONSTRATION OF TYPE-II SINGULARITY

We study the effects an abrupt transition described by the signum function. This description leads to a type-II (sudden) singularity, characterized by

$$t = t_\dagger, \qquad a = a_\dagger < \infty,$$
$$\rho_{\text{tot}}(a_\dagger) < \infty, \qquad |P_{\text{tot}}(a_\dagger)| \to \infty, \qquad \text{(A1)}$$

with the following characteristics: the scale factor $a(t)$ is continuous and nonzero at the moment $t_\dagger$, the first derivative of the scale factor $\dot{a}$ is discontinuous at $t_\dagger$, and its second derivative $\ddot{a}$ diverges at $t_\dagger$ [122]. We prove this argument by considering that $\ddot{a}/a = \dot{H} + H^2$, and by implementing Friedmann equation

$$H^2 = \frac{8\pi G}{3}\tilde{\rho}_{\text{m0}}[a^{-3} + \omega_s \text{sgn}(1/a_\dagger - 1/a)] \quad \text{(A2)}$$
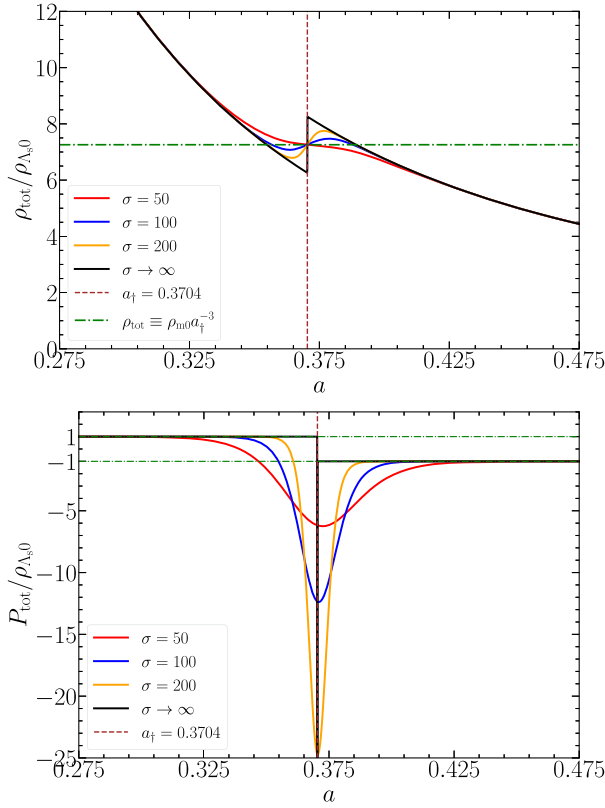
we obtain

FIG. 7.   Total density and total pressure of the Λ_sCDM universe [see Eq. (A5)] with respect to the scale factor. For $\sigma \to \infty$, we observe that $\rho_{\text{tot}}(a_\dagger) \to \text{const} > 0$, while $P_{\text{tot}}(a_\dagger) \to -\infty$. The curves become steeper as the (σ) value increases.

$$\frac{\ddot{a}}{a} = -\frac{4\pi G}{3}\rho_{\text{m0}}[a^{-3} - 2\omega_s \text{sgn}(1/a_\dagger - 1/a) - 2\omega_s a^{-1}\delta(1/a_\dagger - 1/a)], \tag{A3}$$

where δ represents the Dirac delta function. It is evident that at the precise moment of the singularity, $\frac{\ddot{a}}{a} \to \infty$. Given that $P_{\text{tot}} = -\frac{1}{8\pi G}[2\frac{\ddot{a}}{a} + (\frac{\dot{a}}{a})^2]$, at the moment of transition, $P_{\text{tot}} \to -\infty$. This is a feature that can arise in universes with any spatial curvature. Additionally, by resembling a smooth transition, the energy density of Λ_s will be written as follows:

$$\rho_{\Lambda_s}(a) = \rho_{\Lambda_s 0}\frac{\tanh[\sigma(a - a_\dagger)]}{\tanh[\sigma(1 - a_\dagger)]}, \tag{A4}$$

for $\rho_{\Lambda_s 0} > 0$, where $a_\dagger < 1$ and $\sigma > 0$[10] is a parameter determining the rapidity of the transition. Under this parametrization, the total energy density and total pressure of the Universe, containing only dust and Λ_s, can be written as

---

[10]One must set $\sigma \gg 1$ to approximate the signum function.

$$\rho_{\text{tot}}(a) = \rho_{\text{m0}}a^{-3} + \rho_{\Lambda_s 0}\frac{\tanh[\sigma(a - a_\dagger)]}{\tanh[\sigma(1 - a_\dagger)]},$$

$$P_{\text{tot}}(a) = -\rho_{\Lambda_s 0}\left[\frac{\tanh[\sigma(a - a_\dagger)]}{\tanh[\sigma(1 - a_\dagger)]} + \sigma\frac{a}{3}\frac{\text{sech}^2[\sigma(a - a_\dagger)]}{\tanh[\sigma(1 - a_\dagger)]}\right]. \tag{A5}$$

Upon examining the characteristics of $\rho_{\text{tot}}(a)$ and $P_{\text{tot}}(a)$ at $a = a_\dagger$, we find

$$\rho_{\text{tot}}(a_\dagger) = \rho_{\text{m0}}a_\dagger^{-3},$$

$$P_{\text{tot}}(a_\dagger) = -\rho_{\Lambda_s 0}\frac{a}{3}\frac{\sigma}{\tanh[\sigma(1 - a_\dagger)]}. \tag{A6}$$

Notice that $\rho_{\text{tot}}(a_\dagger)$ does not depend on σ, and $P_{\text{tot}}(a_\dagger)$ is negative but finite for finite values of σ (See also Fig. 7).

The "smoothed-out energy density of Λ_s" [Eq. (A6) [reduces, by taking $\sigma \to \infty$, to an abrupt (sudden) AdS $\to$ dS transition, which we study in this paper:

$$\lim_{\sigma \to \infty}\rho_{\Lambda_s}(a) = \rho_{\Lambda_s 0}\text{sgn}[a - a_\dagger]. \tag{A7}$$

In this case, we observe that the total pressure diverges to negative infinity,

$$\lim_{\sigma \to \infty}P_{\text{tot}}(a_\dagger) = -\infty, \tag{A8}$$

while the total energy density remains positive and finite. Thus, this behavior, which occurs at the limit of $\sigma \to \infty$, is characterized by a type-II (sudden) cosmological singularity [122,123]. Note that at the moment when the singularity occurs, the equation of state parameter w_{Λ_s} is undefined; this is a feature of sudden singularities. But even for finite values of σ, i.e., by smoothing out ρ_{Λ_s} (ensuring continuity at ρ_{Λ_s}, which implies it should obtain the zero value at the moment of the transition), where a sudden cosmological singularity won't occur, even then, given that we have assumed the continuity equation $\dot{\rho} + 3H(\rho + p) = 0$ together with an equation of state, we conclude that the right and left limits of the equation of state parameter at the moment of transition will be $w^{(\pm)} \to \pm\infty$. Therefore, the equation of state parameter cannot be defined even for finite σ (see [121]).

APPENDIX B: GRAVITATIONAL POTENTIALS FOR DM AND DE

The Poisson equation for a barotropic fluid, described by $P = w\rho$, is expressed as

$$\nabla^2\Phi = 4\pi G\rho(1 + 3w). \tag{B1}$$

In a theoretical framework where a homogeneous energy density is spherically distributed within a radius R and the

gravitational potential is denoted as $\Phi \equiv \Phi(r)$, the general solution is applied:

$$\Phi(r) = 2\pi G\rho(1+3w)\frac{r^2}{3} - \frac{C}{r} + \mathcal{D}. \tag{B2}$$

The gravitational potential of DM, Φ_{DM}, is determined by assuming $\rho(r > R) = 0$. As a result, the general solution is reformulated as

$$\Phi_{I}(r > R) = 2\pi G\rho(1+3w)\frac{r^2}{3} - \frac{C}{r} + \mathcal{D},$$

$$\Phi_{II}(r < R) = \frac{C}{r} + \mathcal{D}. \tag{B3}$$

The boundary conditions are defined as follows: (a) $\Phi_I(r = 0) < \infty$, (b) $\Phi_{II}(r \to \infty) = 0$, (c) $\Phi_I(r = R) = \Phi_{II}(r = R)$, and (d) $d\Phi_I/dr|_{r=R} = d\Phi_{II}/dr|_{r=R}$. Applying the general solution from Eq. (B3) for the DM density ρ_{DM} (assuming $w_{DM} = 0$) within a sphere of radius R, we obtain

$$\Phi_{DM}(r) = \begin{cases} -2\pi G\rho_{DM}(R^2 - r^2/3), & r \le R, \\ -4\pi G\rho_{DM}R^3/3r, & r \ge R. \end{cases} \tag{B4}$$

Meanwhile, the gravitational potential of DE, Φ_{DE}, is determined by imposing a uniform energy density across the Universe as boundary conditions: (a) $\Phi(r = 0) < \infty$ and (b) $\Phi(r = 0) = 0$. Thus, applying these conditions to Eq. (B2), we deduce that

$$\Phi_{DE}(r) = 2\pi G\rho_{DE}(1 + 3w_{DE})\frac{r^2}{3}. \tag{B5}$$

APPENDIX C: SCALE FACTOR OF THE Λ_sCDM MODEL

To elucidate the scale factor in terms of comoving time, we employ the Friedmann equation, articulated as

$$\frac{H^2}{H_0^2} = \Omega_{m0}a^{-3} + \Omega_{\Lambda_s 0}\mathrm{sgn}(1/a_\dagger - 1/a). \tag{C1}$$

The scale factor maintains continuity and can be characterized by integrating Eq. (C1), as demonstrated below:

$$\dot{a} = H_0[\Omega_{m0}a^{-1} + \Omega_{\Lambda_s 0}a^2\mathrm{sgn}(1/a_\dagger - 1/a)]^{\frac{1}{2}}. \tag{C2}$$

In particular, for $a < a_\dagger$ the integration is given by

$$\int_0^a \frac{da}{(\Omega_{m0}a^{-1} - \Omega_{\Lambda_s 0}a^2)^{\frac{1}{2}}} = H_0 t. \tag{C3}$$

By changing the variable $a = y^{\frac{2}{3}}\left(\frac{1-\Omega_{\Lambda_s 0}}{\Omega_{\Lambda_s 0}}\right)^{\frac{1}{3}}$ and given that $da = \frac{2}{3}\left(\frac{1-\Omega_{\Lambda_s 0}}{\Omega_{\Lambda_s 0}}\right)^{\frac{1}{3}}y^{-\frac{1}{3}}dy$, Eq. (C3) implies

$$a(t) = \left(\frac{1 - \Omega_{\Lambda_s 0}}{\Omega_{\Lambda_s 0}}\right)^{\frac{1}{3}}\sin^{\frac{2}{3}}\left(\frac{3}{2}\sqrt{\Omega_{\Lambda_s 0}}H_0 t\right). \tag{C4}$$

Subsequently, if $a > a_\dagger$, then the integration proceeds as

$$\int_0^{a_\dagger} \frac{da}{(\Omega_{m0}a^{-1} - \Omega_{\Lambda_s 0}a^2)^{\frac{1}{2}}} + \int_{a_\dagger}^a \frac{da}{(\Omega_{m0}a^{-1} + \Omega_{\Lambda_s 0}a^2)^{\frac{1}{2}}} = H_0 t. \tag{C5}$$

In that case, Eq. (C5) implies

$$a(t) = \left(\frac{1 - \Omega_{\Lambda_s 0}}{\Omega_{\Lambda_s 0}}\right)^{\frac{1}{3}}\sinh^{\frac{2}{3}}\left[\frac{3}{2}\sqrt{\Omega_{\Lambda_s 0}}H_0(t - t_\dagger) + \sinh^{-1}\left[\sin\left(\frac{3}{2}\sqrt{\Omega_{\Lambda_s 0}}H_0 t_\dagger\right)\right]\right]. \tag{C6}$$

Subsequently, we get

$$\frac{\ddot{a}}{a} = \begin{cases} -\frac{4}{9}\mathcal{A}_1^2\left[1 + \frac{1}{1-\cos(2\mathcal{A}_1 t)}\right], & t < t_\dagger, \\ -\frac{4}{9}\mathcal{A}_1^2\left[-2 + \frac{1}{\sinh[\mathcal{A}_1(t-t_\dagger)+\mathcal{A}_2]}\right], & t > t_\dagger, \end{cases} \tag{C7}$$

where we have denoted

$$\mathcal{A}_1 \equiv \frac{3}{2}H_0\sqrt{(1 - \Omega_{m0})},$$

$$\mathcal{A}_2 \equiv \sinh^{-1}[\sin(\mathcal{A}_1 t_\dagger)].$$

Next, the general solutions to the free particle geodesic (48) are outlined separately for the two distinct periods of comoving time, $t \ge t_\dagger$ and $t \le t_\dagger$, as follows:

$$r(t) = \begin{cases} \mathcal{C}_1[-1+\cos(\mathcal{A}_1 t)^2]^{\frac{1}{4}}P_{\frac{1}{6}}^{\frac{1}{6}}[\cos(\mathcal{A}_1 t)] \\ +\mathcal{C}_2[-1+\cos(\mathcal{A}_1 t)^2]^{\frac{1}{4}}Q_{\frac{1}{6}}^{\frac{1}{6}}[\cos(\mathcal{A}_1 t)], & t \le t_\dagger, \\ \mathcal{B}\mathcal{D}_1 {}_2F_1\left[-\frac{1}{6},\frac{1}{3},\frac{5}{6},\tanh^2[\mathcal{A}_1(t-t_\dagger)+\mathcal{A}_2]\right] \\ +\mathcal{B}\mathcal{D}_2\tanh^{\frac{2}{3}}[\mathcal{A}_1(t-t_\dagger)+\mathcal{A}_2], & t \ge t_\dagger, \end{cases} \tag{C8}$$

where we have denoted

$$\mathcal{B} \equiv [-1 + \tanh^2(\mathcal{A}_1(t - t_\dagger) + \mathcal{A}_2)]^{-1/2},$$

and P_l^m, Q_l^m represent the associated Legendre functions of the first and second kind, respectively. Meanwhile, ${}_2F_1$ is

the hypergeometric function [166]. The constants are determined through the appropriate boundary conditions.

APPENDIX D: DETERMINING COSMOLOGICAL PARAMETERS

In order to determine the cosmological parameters for our analysis, we follow a method used in [167–169]. The locations of peaks (i.e., peak spacing) in the CMB power spectrum,[11] l_A, are well-measured quantities and are defined as

$$l_A \equiv \pi(1+z_*)\frac{D_A(z_*)}{r_s^*} = \frac{\pi}{\theta_s^*}, \qquad (D1)$$

where $\theta_s^* \equiv r_s^*/d_A(z_*)$ represents the angular size of the sound horizon at the last-scattering surface [170–172]. Here, r_s^* represents the comoving sound horizon at the last-scattering surface:

$$r_s^* = \int_{z_*}^{\infty} c_s(z)\frac{\mathrm{d}z}{H(z)}, \qquad (D2)$$

where $c_s(z)$ is the sound speed of the photon-baryon fluid,

$$c_s(z) = \frac{c}{\sqrt{3(1+\frac{3\omega_b}{4\omega_\gamma(1+z)})}}, \qquad (D3)$$

and z_* is the redshift at the last-scattering surface, which can be approximated analytically via [173]

$$z_* = 1048[1+0.00124(\omega_b)^{-0.738}][1+g_1(\omega_m)^{g_2}],$$
$$g_1 = 0.0783(\omega_b)^{-0.238}[1+39.5(\omega_b)^{0.763}]^{-1},$$
$$g_2 = 0.560[1+21.1(\omega_b)^{1.81}]^{-1}. \qquad (D4)$$

Meanwhile, the proper angular diameter distance to the last-scattering surface is defined as

$$D_A(z_*) \equiv \frac{d_A(z_*)}{1+z_*} = \frac{c}{1+z_*}\int_0^{z_*}\frac{\mathrm{d}z}{H(z)}. \qquad (D5)$$

In what follows, we start the calculations by assuming that the acoustic scale and the physical density parameter for matter in the ΛCDM Universe will be equal to the Λ_sCDM

---

[11]Also known as the "acoustic scales."

TABLE II. Plik best-fit values taken from the *Planck* 2018 data set [4]. We define the physical radiation density parameter as the sum of the physical photon and neutrino density parameters, $\omega_r \equiv \omega_\gamma + \omega_n = 2.469 \times 10^{-5} \times [1 + \frac{7}{8}(\frac{4}{11})^{4/3}N_{\text{eff}}]$, with $N_{\text{eff}} = 3.046$ for the standard model of particle physics.

Parameter	Value
ω_b	0.022383
ω_m	0.143140
ω_r	4.177×10^{-5}
$100\theta_s^*$	1.041085

model[12] (i.e., $l_A^\Lambda \simeq l_A^{\Lambda_s}$ and $\omega_m^\Lambda \simeq \omega_m^{\Lambda_s}$). Since Λ_sCDM does not change N_{eff} or the physics of the early Universe, we can further assume that $\omega_r^\Lambda \simeq \omega_r^{\Lambda_s}$ and $\omega_b^\Lambda \simeq \omega_b^{\Lambda_s}$.

Under these conditions, z_* and $c_s(z)$ will be the same for the ΛCDM and Λ_sCDM models, which can be seen via Eqs. (D3) and (D4). By combining Eqs. (D1), (D2), and (D5), we can write

$$\theta_s^* = \frac{\int_{z_*}^{\infty}\frac{c_s(z)\mathrm{d}z}{\sqrt{\omega_m(1+z)^3+\omega_r(1+z)^4+(h_0^2-\omega_m-\omega_r)f_{\text{DE}}(z)}}}{\int_0^{z_*}\frac{c\mathrm{d}z}{\sqrt{\omega_m(1+z)^3+\omega_r(1+z)^4+(h_0^2-\omega_m-\omega_r)f_{\text{DE}}(z)}}}. \qquad (D6)$$

Since the value of the parameter θ_s^* is fixed by *Planck* CMB observations almost model independently, we can constrain h_0 for any given $f_{\text{DE}}(z) \equiv \rho_{\text{DE}}(z)/\rho_{\text{DE},0}$ [viz., $f_\Lambda(z) \equiv 1$ and $f_{\Lambda_s}(z) \equiv \text{sgn}(z_\dagger - z)$], provided the pre-recombination Universe remains as in the standard cosmological model.

To simplify the above procedure, one can use the fitting formulas given below to calculate the Ω_{m0} for the Λ_sCDM model, expressed in terms of the transition redshift, $z_\dagger$:

$$\Omega_{m0}(z_\dagger) = c_0 + c_1 z_\dagger^{-1} + c_2 z_\dagger^{-2} + c_3 z_\dagger^{-3}. \qquad (D7)$$

By assuming the Table II parameters, we obtain the constants of the equation as $(c_0, c_1, c_2, c_3) = (0.3093, 0.0155, -0.0994, -0.0722)$, which correctly finds Ω_{m0} up to the order of 10^{-4} for $1.5 \leq z_\dagger \leq 11.5$.

---

[12]CMB distance priors, l_A and R, (viz., ω_m) are actually derived parameters by fitting a cosmological model to the CMB power spectra [174–176]. Thus, the underlying cosmology would change the distance priors [177]. Since Λ_sCDM does not change the physics of the early Universe, we can assume that it will not cause a significant variation in l_A or ω_m.

[1] S. Dodelson and F. Schmidt, *Modern Cosmology*, 2nd ed. (Academic Press, New York, 2021), pp. 1–19.

[2] A. G. Riess *et al.* (Supernova Search Team Collaboration), Astron. J. **116,** 1009 (1998).

[3] S. Perlmutter *et al.* (Supernova Cosmology Project Collaboration), Astrophys. J. **517,** 565 (1999).

[4] N. Aghanim *et al.* (Planck Collaboration), Astron. Astrophys. **641,** A6 (2020); **652,** C4(E) (2021).

[5] S. Aiola *et al.* (ACT Collaboration), J. Cosmol. Astropart. Phys. 12 (2020) 047.

[6] S. Alam *et al.* (eBOSS Collaboration), Phys. Rev. D **103,** 083533 (2021).

[7] M. Asgari *et al.* (KiDS Collaboration), Astron. Astrophys. **645,** A104 (2021).

[8] T. M. C. Abbott *et al.* (DES Collaboration), Phys. Rev. D **105,** 023520 (2022).

[9] S. Weinberg, Rev. Mod. Phys. **61,** 1 (1989).

[10] S. M. Carroll, W. H. Press, and E. L. Turner, Annu. Rev. Astron. Astrophys. **30,** 499 (1992).

[11] V. Sahni and A. A. Starobinsky, Int. J. Mod. Phys. D **09,** 373 (2000).

[12] P. J. E. Peebles and B. Ratra, Rev. Mod. Phys. **75,** 559 (2003).

[13] T. Padmanabhan, Phys. Rep. **380,** 235 (2003).

[14] P. Bull *et al.*, Phys. Dark Universe **12,** 56 (2016).

[15] E. Di Valentino *et al.*, Astropart. Phys. **131,** 102605 (2021).

[16] E. Di Valentino, O. Mena, S. Pan, L. Visinelli, W. Yang, A. Melchiorri, D. F. Mota, A. G. Riess, and J. Silk, Classical Quantum Gravity **38,** 153001 (2021).

[17] P. J. E. Peebles, Ann. Phys. (Amsterdam) **447,** 169159 (2022).

[18] L. Perivolaropoulos and F. Skara, New Astron. Rev. **95,** 101659 (2022).

[19] E. Abdalla *et al.*, J. High Energy Astrophys. **34,** 49 (2022).

[20] S. Vagnozzi, Universe **9,** 393 (2023).

[21] J.-P. Hu and F.-Y. Wang, Universe **9,** 94 (2023).

[22] O. Akarsu, E. O. Colgáin, A. A. Sen, and M. M. Sheikh-Jabbari, arXiv:2402.04767.

[23] A. G. Riess *et al.*, Astrophys. J. Lett. **934,** L7 (2022).

[24] P. A. Burger *et al.*, Astron. Astrophys. **683,** A103 (2024).

[25] S.-F. Chen, Z. Vlah, and M. White, J. Cosmol. Astropart. Phys. 02 (2022) 008.

[26] S. A. Adil, O. Akarsu, M. Malekjani, E. O. Colgáin, S. Pourojaghi, A. A. Sen, and M. M. Sheikh-Jabbari, Mon. Not. R. Astron. Soc. **528,** L20 (2023).

[27] T. Karwal and M. Kamionkowski, Phys. Rev. D **94,** 103523 (2016).

[28] V. Poulin, T. L. Smith, T. Karwal, and M. Kamionkowski, Phys. Rev. Lett. **122,** 221301 (2019).

[29] V. Poulin, T. L. Smith, D. Grin, T. Karwal, and M. Kamionkowski, Phys. Rev. D **98,** 083525 (2018).

[30] P. Agrawal, F.-Y. Cyr-Racine, D. Pinner, and L. Randall, Phys. Dark Universe **42,** 101347 (2023).

[31] M. Kamionkowski and A. G. Riess, Annu. Rev. Nucl. Part. Sci. **73,** 153 (2023).

[32] S. D. Odintsov, V. K. Oikonomou, and G. S. Sharov, Phys. Lett. B **843,** 137988 (2023).

[33] F. Niedermann and M. S. Sloth, Phys. Rev. D **103,** L041303 (2021).

[34] J. S. Cruz, F. Niedermann, and M. S. Sloth, J. Cosmol. Astropart. Phys. 11 (2023) 033.

[35] F. Niedermann and M. S. Sloth, arXiv:2307.03481.

[36] G. Ye and Y.-S. Piao, Phys. Rev. D **101,** 083507 (2020).

[37] G. Ye and Y.-S. Piao, Phys. Rev. D **102,** 083523 (2020).

[38] G. Ye, J. Zhang, and Y.-S. Piao, Phys. Lett. B **839,** 137770 (2023).

[39] M. Rossi, M. Ballardini, M. Braglia, F. Finelli, D. Paoletti, A. A. Starobinsky, and C. Umiltà, Phys. Rev. D **100,** 103524 (2019).

[40] M. Braglia, M. Ballardini, W. T. Emond, F. Finelli, A. E. Gumrukcuoglu, K. Koyama, and D. Paoletti, Phys. Rev. D **102,** 023529 (2020).

[41] T. Adi and E. D. Kovetz, Phys. Rev. D **103,** 023530 (2021).

[42] M. Braglia, M. Ballardini, F. Finelli, and K. Koyama, Phys. Rev. D **103,** 043528 (2021).

[43] M. Ballardini, M. Braglia, F. Finelli, D. Paoletti, A. A. Starobinsky, and C. Umiltà, J. Cosmol. Astropart. Phys. 10 (2020) 044.

[44] G. Franco Abellán, M. Braglia, M. Ballardini, F. Finelli, and V. Poulin, J. Cosmol. Astropart. Phys. 12 (2023) 017.

[45] M. Petronikolou and E. N. Saridakis, Universe **9,** 397 (2023).

[46] D. K. Hazra, A. Antony, and A. Shafieloo, J. Cosmol. Astropart. Phys. 08 (2022) 063.

[47] O. Akarsu, J. D. Barrow, L. A. Escamilla, and J. A. Vazquez, Phys. Rev. D **101,** 063528 (2020).

[48] O. Akarsu, S. Kumar, E. Özülker, and J. A. Vazquez, Phys. Rev. D **104,** 123512 (2021).

[49] O. Akarsu, S. Kumar, E. Özülker, J. A. Vazquez, and A. Yadav, Phys. Rev. D **108,** 023513 (2023).

[50] O. Akarsu, E. Di Valentino, S. Kumar, R. C. Nunes, J. A. Vazquez, and A. Yadav, arXiv:2307.10899.

[51] E. Di Valentino, A. Mukherjee, and A. A. Sen, Entropy **23,** 404 (2021).

[52] G. Alestas, L. Kazantzidis, and L. Perivolaropoulos, Phys. Rev. D **101,** 123516 (2020).

[53] G. Alestas, L. Kazantzidis, and L. Perivolaropoulos, Phys. Rev. D **103,** 083517 (2021).

[54] M. R. Gangopadhyay, S. K. J. Pacif, M. Sami, and M. K. Sharma, Universe **9,** 83 (2023).

[55] S. Basilakos, A. Lymperis, M. Petronikolou, and E. N. Saridakis, Eur. Phys. J. C **84,** 297 (2024).

[56] S. A. Adil, O. Akarsu, E. Di Valentino, R. C. Nunes, E. Özülker, A. A. Sen, and E. Specogna, Phys. Rev. D **109,** 023527 (2024).

[57] M. R. Gangopadhyay, M. Sami, and M. K. Sharma, Phys. Rev. D **108,** 103526 (2023).

[58] L. Visinelli, S. Vagnozzi, and U. Danielsson, Symmetry **11,** 1035 (2019).

[59] K. Dutta, Ruchika, A. Roy, A. A. Sen, and M. M. Sheikh-Jabbari, Gen. Relativ. Gravit. **52,** 15 (2020).

[60] A. A. Sen, S. A. Adil, and S. Sen, Mon. Not. R. Astron. Soc. **518,** 1098 (2022).

[61] S. Kumar and R. C. Nunes, Phys. Rev. D **96,** 103511 (2017).

[62] E. Di Valentino, A. Melchiorri, and O. Mena, Phys. Rev. D **96,** 043503 (2017).

[63] W. Yang, A. Mukherjee, E. Di Valentino, and S. Pan, Phys. Rev. D **98**, 123527 (2018).

[64] S. Pan, W. Yang, E. Di Valentino, E. N. Saridakis, and S. Chakraborty, Phys. Rev. D **100**, 103520 (2019).

[65] S. Kumar, R. C. Nunes, and S. K. Yadav, Eur. Phys. J. C **79**, 576 (2019).

[66] E. Di Valentino, A. Melchiorri, O. Mena, and S. Vagnozzi, Phys. Rev. D **101**, 063502 (2020).

[67] E. Di Valentino, A. Melchiorri, O. Mena, and S. Vagnozzi, Phys. Dark Universe **30**, 100666 (2020).

[68] M. Lucca and D. C. Hooper, Phys. Rev. D **102**, 123502 (2020).

[69] A. Gómez-Valent, V. Pettorino, and L. Amendola, Phys. Rev. D **101**, 123513 (2020).

[70] S. Kumar, Phys. Dark Universe **33**, 100862 (2021).

[71] R. C. Nunes, S. Vagnozzi, S. Kumar, E. Di Valentino, and O. Mena, Phys. Rev. D **105**, 123506 (2022).

[72] A. Bernui, E. Di Valentino, W. Giarè, S. Kumar, and R. C. Nunes, Phys. Rev. D **107**, 103531 (2023).

[73] E. Aubourg *et al.*, Phys. Rev. D **92**, 123516 (2015).

[74] V. Sahni, A. Shafieloo, and A. A. Starobinsky, Astrophys. J. Lett. **793**, L40 (2014).

[75] V. Poulin, K. K. Boddy, S. Bird, and M. Kamionkowski, Phys. Rev. D **97**, 123504 (2018).

[76] Y. Wang, L. Pogosian, G.-B. Zhao, and A. Zucca, Astrophys. J. Lett. **869**, L8 (2018).

[77] A. Bonilla, S. Kumar, and R. C. Nunes, Eur. Phys. J. C **81**, 127 (2021).

[78] L. A. Escamilla, O. Akarsu, E. Di Valentino, and J. A. Vazquez, J. Cosmol. Astropart. Phys. 11 (2023) 051.

[79] L. A. Escamilla and J. A. Vazquez, Eur. Phys. J. C **83**, 251 (2023).

[80] M. Malekjani, R. M. Conville, E. O. Colgáin, S. Pourojaghi, and M. M. Sheikh-Jabbari, arXiv:2301.12725.

[81] O. Akarsu, E. O. Colgain, E. Özulker, S. Thakur, and L. Yin, Phys. Rev. D **107**, 123526 (2023).

[82] R. Calderón, R. Gannouji, B. L'Huillier, and D. Polarski, Phys. Rev. D **103**, 023526 (2021).

[83] V. Marra and L. Perivolaropoulos, Phys. Rev. D **104**, L021303 (2021).

[84] G. Alestas, I. Antoniou, and L. Perivolaropoulos, Universe **7**, 366 (2021).

[85] G. Alestas, D. Camarena, E. Di Valentino, L. Kazantzidis, V. Marra, S. Nesseris, and L. Perivolaropoulos, Phys. Rev. D **105**, 063538 (2022).

[86] L. Perivolaropoulos and F. Skara, Phys. Rev. D **104**, 123511 (2021).

[87] S. Pan, O. Seto, T. Takahashi, and Y. Toda, arXiv:2312.15435.

[88] K. Naidoo, M. Jaber, W. A. Hellwing, and M. Bilicki, arXiv:2209.08102.

[89] M. Boylan-Kolchin, Nat. Astron. **7**, 731 (2023).

[90] I. Labbé, P. van Dokkum, E. Nelson, R. Bezanson, K. A. Suess, J. Leja, G. Brammer, K. Whitaker, E. Mathews, M. Stefanon, and B. Wang, Nature (London) **616**, 266 (2023).

[91] N. Menci, M. Castellano, P. Santini, E. Merlin, A. Fontana, and F. Shankar, Astrophys. J. Lett. **938**, L5 (2022).

[92] M. Biagetti, G. Franciolini, and A. Riotto, Astrophys. J. **944**, 113 (2023).

[93] M. Forconi, Ruchika, A. Melchiorri, O. Mena, and N. Menci, J. Cosmol. Astropart. Phys. 10 (2023) 012.

[94] R. P. Gupta, Mon. Not. R. Astron. Soc. **524**, 3385 (2023).

[95] K. Glazebrook *et al.*, arXiv:2308.05606.

[96] S. A. Adil, U. Mukhopadhyay, A. A. Sen, and S. Vagnozzi, J. Cosmol. Astropart. Phys. 10 (2023) 072.

[97] S. Hirano and N. Yoshida, Astrophys. J. **963**, 2 (2024).

[98] P. Parashari and R. Laha, Mon. Not. R. Astron. Soc. **526**, L63 (2023).

[99] L. Y. A. Yung, R. S. Somerville, S. L. Finkelstein, S. M. Wilkins, and J. P. Gardner, Mon. Not. R. Astron. Soc. **527**, 5929 (2023).

[100] J. McCaffrey, S. Hardin, J. Wise, and J. Regan, Open J. Astrophys. **6** (2023), 10.21105/astro.2304.13755.

[101] Y.-Y. Wang, L. Lei, G.-W. Yuan, and Y.-Z. Fan, Astrophys. J. Lett. **954**, L48 (2023).

[102] J. Wang, Z. Huang, L. Huang, and J. Liu, Res. Astron. Astrophys. **24**, 045001 (2024).

[103] D. Wang and Y. Liu, arXiv:2301.00347.

[104] F. Melia, Mon. Not. R. Astron. Soc. **521**, L85 (2023).

[105] E. A. Paraskevas and L. Perivolaropoulos, arXiv:2308.07046.

[106] N. Menci, S. A. Adil, U. Mukhopadhyay, A. A. Sen, and S. Vagnozzi, arXiv:2401.12659.

[107] L. Kazantzidis and L. Perivolaropoulos, *Modified Gravity and Cosmology* (Springer, Cham, 2021).

[108] D. Benisty, Phys. Dark Universe **31**, 100766 (2021).

[109] R. C. Nunes and S. Vagnozzi, Mon. Not. R. Astron. Soc. **505**, 5427 (2021).

[110] S. Bocquet *et al.* (SPT Collaboration), Astrophys. J. **878**, 55 (2019).

[111] J. M. Maldacena, Adv. Theor. Math. Phys. **2**, 231 (1998).

[112] R. Bousso and J. Polchinski, J. High Energy Phys. 06 (2000) 006.

[113] L. A. Anchordoqui, I. Antoniadis, and D. Lust, arXiv:2312.12352.

[114] B. Alexandre, S. Gielen, and J. a. Magueijo, J. Cosmol. Astropart. Phys. 02 (2024) 036.

[115] O. Akarsu, A. De Felice, E. Di Valentino, S. Kumar, R. C. Nunes, E. Ozulker, J. A. Vazquez, and A. Yadav, arXiv:2402.07716.

[116] A. De Felice, A. Doll, and S. Mukohyama, J. Cosmol. Astropart. Phys. 09 (2020) 034.

[117] A. De Felice, S. Mukohyama, and M. C. Pookkillath, Phys. Lett. B **816**, 136201 (2021); **818**, 136364(E) (2021).

[118] J. Garriga, A. D. Linde, and A. Vilenkin, Phys. Rev. D **69**, 063521 (2004).

[119] J. Garriga, L. Pogosian, and T. Vachaspati, Phys. Rev. D **69**, 063511 (2004).

[120] L. Perivolaropoulos, Phys. Rev. D **71**, 063503 (2005).

[121] E. Ozulker, Phys. Rev. D **106**, 063509 (2022).

[122] J. D. Barrow, Classical Quantum Gravity **21**, L79 (2004).

[123] S. Nojiri, S. D. Odintsov, and S. Tsujikawa, Phys. Rev. D **71**, 063004 (2005).

[124] L. Fernandez-Jambrina and R. Lazkoz, Phys. Rev. D **74**, 064030 (2006).

[125] A. Balcerzak, T. Denkiewicz, and M. Lisaj, Eur. Phys. J. C **83**, 980 (2023).

[126] J. de Haro, S. Nojiri, S. D. Odintsov, V. K. Oikonomou, and S. Pan, Phys. Rep. **1034**, 1 (2023).

[127] O. Trivedi, arXiv:2309.08954.

[128] E. A. Paraskevas and L. Perivolaropoulos, Universe **9**, 317 (2023).

[129] V. R. Eke, S. Cole, and C. S. Frenk, Mon. Not. R. Astron. Soc. **282**, 263 (1996).

[130] E. L. Lokas and Y. Hoffman, *The Identification of Dark Matter* (World Scientific, Singapore, 2001).

[131] D. F. Mota and C. van de Bruck, Astron. Astrophys. **421**, 71 (2004).

[132] P. Creminelli, G. D'Amico, J. Norena, L. Senatore, and F. Vernizzi, J. Cosmol. Astropart. Phys. 03 (2010) 027.

[133] V. Pavlidou and B. D. Fields, Phys. Rev. D **71**, 043510 (2005).

[134] C. Horellou and J. Berge, Mon. Not. R. Astron. Soc. **360**, 1393 (2005).

[135] S. Basilakos, Astrophys. J. **590**, 636 (2003).

[136] D. Tanoglidis, V. Pavlidou, and T. Tomaras, J. Cosmol. Astropart. Phys. 12 (2015) 060.

[137] D. Tanoglidis, V. Pavlidou, and T. Tomaras, arXiv: 1601.03740.

[138] F. Pace, S. Meyer, and M. Bartelmann, J. Cosmol. Astropart. Phys. 10 (2017) 040.

[139] V. Pavlidou, G. Korkidis, T. Tomaras, and D. Tanoglidis, Astron. Astrophys. **638**, L8 (2020).

[140] W. H. Press and P. Schechter, Astrophys. J. **187**, 425 (1974).

[141] J. R. Bond, S. Cole, G. Efstathiou, and N. Kaiser, Astrophys. J. **379**, 440 (1991).

[142] A. Cooray and R. K. Sheth, Phys. Rep. **372**, 1 (2002).

[143] M. Asgari, A. J. Mead, and C. Heymans, Open J. Astrophys. **6** (2023), 10.21105/astro.2303.08752.

[144] S. Dodelson and F. Schmidt, in *Modern Cosmology (Second Edition)*, edited by S. Dodelson and F. Schmidt (Academic Press, New York, 2021), pp. 325–372.

[145] G. A. Baker, Jr., Gen. Relativ. Gravit. **34**, 767 (2001).

[146] S. Nesseris and L. Perivolaropoulos, Phys. Rev. D **70**, 123529 (2004).

[147] V. Faraoni and A. Jacques, Phys. Rev. D **76**, 063510 (2007).

[148] L. Perivolaropoulos, Phys. Rev. D **94**, 124018 (2016).

[149] O. Lahav, P. B. Lilje, J. R. Primack, and M. J. Rees, Mon. Not. R. Astron. Soc. **251**, 128 (1991).

[150] I. T. Iliev and P. R. Shapiro, Mon. Not. R. Astron. Soc. **325**, 468 (2001).

[151] I. Maor and O. Lahav, J. Cosmol. Astropart. Phys. 07 (2005) 003.

[152] P. Saha, D. Dey, and K. Bhattacharya, Phys. Rev. D **108**, 084025 (2023).

[153] R. A. Battye and J. Weller, Phys. Rev. D **68**, 083506 (2003).

[154] L.-M. Wang and P. J. Steinhardt, Astrophys. J. **508**, 483 (1998).

[155] N. N. Weinberg and M. Kamionkowski, Mon. Not. R. Astron. Soc. **341**, 251 (2003).

[156] A. Einstein and E. G. Straus, Rev. Mod. Phys. **17**, 120 (1945).

[157] R. Nandra, A. N. Lasenby, and M. P. Hobson, Mon. Not. R. Astron. Soc. **422**, 2931 (2012).

[158] R. Nandra, A. N. Lasenby, and M. P. Hobson, Mon. Not. R. Astron. Soc. **422**, 2945 (2012).

[159] M. Bouhmadi-López, C.-Y. Chen, and P. Chen, Eur. Phys. J. C **75**, 90 (2015).

[160] I. Antoniou and L. Perivolaropoulos, Phys. Rev. D **93**, 123520 (2016).

[161] A. Kravtsov and S. Borgani, Annu. Rev. Astron. Astrophys. **50**, 353 (2012).

[162] J. Gao, H. Zou, X. Zhou, and X. Kong, Publ. Astron. Soc. Pac. **132**, 024101 (2020).

[163] D. Harvey, A. Robertson, S.-I. Tam, M. Jauzac, R. Massey, J. Rhodes, and I. G. McCarthy, Mon. Not. R. Astron. Soc. **500**, 2627 (2020).

[164] L. Fernandez, M. M. Cueli, J. González-Nuevo, L. Bonavera, D. Crespo, J. M. Casas, and A. Lapi, Astron. Astrophys. **658**, A19 (2022).

[165] S. Sankhyayan, J. Bagchi, E. Tempel, S. More, M. Einasto, P. Dabhade, S. Raychaudhury, R. Athreya, and P. Heinämäki, Astrophys. J. **958**, 62 (2023).

[166] G. Arfken, H. Weber, and F. Harris, *Mathematical Methods for Physicists: A Comprehensive Guide* (Elsevier Science, New York, 2012).

[167] L. Knox and M. Millea, Phys. Rev. D **101**, 043533 (2020).

[168] P. Shah, P. Lemos, and O. Lahav, Astron. Astrophys. Rev. **29**, 9 (2021).

[169] S. Vagnozzi, Phys. Rev. D **102**, 023518 (2020).

[170] E. Komatsu *et al.* (WMAP Collaboration), Astrophys. J. Suppl. Ser. **180**, 330 (2009).

[171] E. Komatsu *et al.*, Astrophys. J. Suppl. Ser. **192**, 18 (2011).

[172] Y. Wang and P. Mukherjee, Phys. Rev. D **76**, 103533 (2007).

[173] W. Hu and N. Sugiyama, Astrophys. J. **471**, 542 (1996).

[174] Y. Wang and S. Wang, Phys. Rev. D **88**, 043522 (2013); **88**, 069903(E) (2013).

[175] Q.-G. Huang, K. Wang, and S. Wang, J. Cosmol. Astropart. Phys. 12 (2015) 022.

[176] L. Chen, Q.-G. Huang, and K. Wang, J. Cosmol. Astropart. Phys. 02 (2019) 028.

[177] O. Elgaroy and T. Multamaki, Astron. Astrophys. **471**, 65 (2007).